EarthArXiv Coversheet

Hybrid Physics–AI Ecosystem Simulations Improve Biogeochemical Predictions in Temperate Shelf Seas

Authors

Deep S. Banerjee[12]*
Jerry Blackford[1]
Gemma Kulk[12]
Shubha Sathyendranath[12]
Jorn Bruggeman[13]
Elin Meek[1]
Heather A. Bouman[4]

Affiliations

[1] Plymouth Marine Laboratory, United Kingdom
[2] National Centre for Earth Observation, United Kingdom
[3] Bolding & Bruggeman ApS, Denmark
[4] Department of Earth Sciences, University of Oxford, United Kingdom

Corresponding Author

Deep S. Banerjee
Email: dba@pml.ac.uk

Preprint Status Statement

This manuscript is a **non-peer-reviewed preprint** submitted to **EarthArXiv**.
The manuscript is **currently under consideration for peer review at *Nature Communications***.

Hybrid Physics–AI Ecosystem Simulations Improve Biogeochemical Predictions in Temperate Shelf Seas

Deep S. Banerjee[1,2*], Jerry Blackford[1], Gemma Kulk[1,2], Shubha Sathyendranath[1,2], Jorn Bruggeman[1,3], Elin Meek[1], Heather A. Bouman[4]

[1]Plymouth Marine Laboratory, United Kingdom.
[2]National Centre for Earth Observation, United Kingdom.
[3]Bolding & Bruggeman ApS, Denmark.
[4]Department of Earth Sciences, University of Oxford, United Kingdom.

*Corresponding author(s). E-mail(s): dba@pml.ac.uk;

Abstract

Biogeochemical models form a core part of marine forecasting and climate projections, yet they suffer from persistent biases in predicting key ecosystem variables, creating challenges across regional and global scales. To address this, we developed an AI-augmented three-dimensional hybrid framework that integrates machine-learning corrections directly into a process-based model's productivity engine at runtime, keeping mechanistic formulations central while deploying physics-constrained, data-driven AI adjustments around them. We explored two independent hybrid pathways: a satellite-trained primary production scale-factor and a physiology-informed parameter adjustment. Using a temperate shelf-sea as a testbed, we evaluated multi-year hybrid simulations against in situ, Argo, and satellite observations, as well as data-assimilative (DA) reanalysis and high-resolution simulations. Results show that the hybrid framework substantially reduced long-standing biases and outperformed reanalysis and high-resolution simulations across several metrics, including evaluation years and variables, not seen during AI training. This demonstrates that correcting ecosystem process representations while remaining mass-conservative can yield greater accuracy than increasing spatial resolution or relying entirely on continuous DA. Furthermore, because our AI components utilise globally available satellite and experimental datasets, our framework is potentially transferable across global shelf seas. This low-computational, interpretable approach could

deliver an effective alternative for operational forecasting and long-term climate applications.

Keywords: Marine biogeochemistry, Hybrid modelling, Physics–AI integration, Primary production, Shelf-sea ecosystems, Operational ocean forecasting, Climate-relevant ecosystem prediction, Earth system modelling

1 Introduction

Accurate biogeochemical forecasting is essential for credible projections of primary production, carbon export, nutrient drawdown and oxygen dynamics to inform climate assessments and marine management decisions. Yet, process-based marine ecosystem models, which underpin biogeochemical forecasting systems, suffer from persistent seasonal and spatial biases in key ecosystem variables such as chlorophyll, nutrients, and dissolved oxygen. These limitations are widely recognised across regional and global domains, as simplified mechanistic formulations struggle to represent the full complexity and variability of real ecosystems. For instance, Andrews et al. (2017) [1] reported difficulties reproducing the observed oxygen levels, particularly in low-latitude oceans, in global Earth System Models, failing to capture the extent and variability of oxygen minimum zones. Yool et al. (2021) [2] further identified biases in UKSEM1 Earth System Models in nutrients and dissolved inorganic carbon in future climate scenarios. In a North American coastal study, the baseline simulation showed a consistent bias where the model underestimated chlorophyll while overestimating nutrients and CO_2 levels across multiple coastal regions [3].

One core source of this structural shortcoming is that physiological parameters and key process formulations are typically prescribed *a priori* and applied homogeneously across seasons and model domains. Whereas phytoplankton communities undergo seasonal succession, acclimation, and shifts in dominant functional traits in response to changes in light, nutrients, and mixing, making fixed physiological parameters difficult to justify. Consistent with this, Mamnun et al. (2025) [4] showed that spatio-temporally constant parameters can introduce substantial uncertainty and bias in marine ecosystem simulations. A conventional response to address this issue is to apply data assimilation (DA). However, assimilating satellite-derived, functional-type-specific phytoplankton information into process-based models [5] demonstrably improves surface chlorophyll and bloom onset, but typically has a more limited impact on the underlying primary production dynamics and nutrient pathways. Moreover, DA approaches that constrain model state variables without fully consistent balance schemes can violate strict carbon, nitrogen and phosphorus (C/N/P) mass conservation (and associated O_2 stoichiometry), potentially introducing inconsistencies in coupled nutrient and carbon cycles while leaving the underlying process rates imperfect, as highlighted by Ciavatta et al. (2014) [6] and Teruzzi et al. (2018) [7]. Consistent with this, Gregg et al. (2008) [8] demonstrated that model chlorophyll responded to assimilated chlorophyll, while carbon remained biased. They highlighted that ocean-colour sensors measure chlorophyll as a proxy for biomass, but do not directly constrain carbon stocks or biogeochemical fluxes. Mateus et al. (2012) [9] and Stock et al. (2025) [10] further reported that large chlorophyll changes can occur with minimal change

in carbon fixation. In simple terms, with assimilation of just the biomass of the pigment chlorophyll-a derived from ocean-colour, we are "painting the right amount of green" at the ocean surface, whilst the underlying engine of marine ecosystem, i.e., the primary productivity that links light, nutrient and carbon flux [11], remains biased, resulting in persistent errors in bloom timing [12], nutrient drawdown and oxygen distributions [13].

Recent work across climate, ocean and environmental modelling shows that combining machine learning (ML) algorithms within physical models yields promising results in terms of both prediction accuracy and stability [14–16]. For biogeochemistry, where biological processes are inherently complex, non-linear, and subject to substantial uncertainty, such an approach would provide a pragmatic way to represent unresolved physiological responses under changing optical conditions, nutrient regimes and mixing environments without altering established process-based formulations. This aligns well with the wider demand for human-guided, augmentation-based uses of Artificial Intelligence (AI)/ML in marine ecosystem modelling, where data-driven methods improve, rather than replace, process understanding and model integrity [17, 18].

In this study, we developed a full three-dimensional hybrid modelling framework that applies machine-learned corrections to the productivity engine of a process-based ecosystem model at runtime, improving the representation of shelf-sea biogeochemistry without altering the underlying physics or model configuration. We used the North West European Shelf (NWES) domain as our experimental testbed, implemented on the Atlantic Margin Model (AMM7) configuration, with a spatial resolution of approximately 7 km and spanning roughly 40°N–65°N and 20°W–13°E. This domain is known to be challenging for simulating complex shelf-sea biogeochemistry and exhibits substantial documented biases in both baseline NEMO (Nucleus for European Modelling of the Ocean)–ERSEM (European Regional Seas Ecosystem Model) [19, 20] and its Copernicus Marine Environment Monitoring Service (CMEMS) NWES biogeochemical reanalysis counterpart [13]. The NWES domain combines strong seasonal variability, tidal mixing fronts, and riverine nutrient loads, making it a particularly challenging testbed for simulating shelf-sea biogeochemistry.

Two independent hybrid pathways are developed in this work. The first comprises an AI/ML model trained on a scale factor derived from the ratio between satellite-based productivity estimates [21–23] and an independent baseline NEMO–ERSEM simulation of primary production [24]. After training, the ML model is coupled online to NEMO–ERSEM to dynamically adjust productivity rates using internally available environmental predictors. This approach is referred to as HYB-SF (hybrid scale-factor correction). Conversely, the second pathway implements online prediction of photosynthesis–irradiance (PI) parameters, using a separate AI/ML model trained on a global experimental dataset of Bouman et al. 2018 [25] and coupled to NEMO-ERSEM, allowing the light-response curve to adjust dynamically to local environmental conditions during model integration. This approach is referred to as HYB-PI (hybrid PI correction). In both pathways, model training and the subsequent online AI-driven corrections during NEMO–ERSEM integration were confined to shelf regions (water depth $\leq$200 m), consistent with the intended shelf-sea application and they both acted exclusively on productivity rates and physiological response parameters, while all carbon, nutrient, and oxygen fluxes remain governed by the native ERSEM stoichiometric formulations, thereby preserving internal mass conservation

by construction. A third simulation using the baseline ERSEM configuration without AI augmentation was performed as a reference (legacy ERSEM). All simulations shared identical physics, initial conditions, grid, and configuration, differing only in the internal treatment of primary production. The isolation is important as primary production is one of the major ecosystem drivers that governs the entire lower-trophic strata of biogeochemical processes: phytoplankton bloom, nutrient drawdown, oxygen dynamics and consumption through respiration [26, 27]. By modifying only this process, we directly assess whether an adaptive primary production engine leads to a more realistic ecosystem state.

We demonstrated that our hybrid framework improved chlorophyll distributions and reduced long-standing biases in surface and subsurface oxygen present in the legacy ERSEM, when evaluated against the North Sea Biogeochemical Climatology (NSBC) level-2 products [28], independent observations, including two different satellite ocean-colour products [29, 30], biogeochemical (BGC) Argo profiles [31], and in situ oxygen and nitrate measurements from International Council for the Exploration of the Sea (ICES) [32]. Performance is further assessed relative to both a data-assimilative biogeochemical reanalysis on the AMM7 grid [13] and a free-running high-resolution regional model over the same NWES domain (AMM15; 1.5 km; 45°N–63°N) [33]. We showed our best-performing hybrid model, HYB-SF, substantially reduced long-standing biases in chlorophyll and dissolved oxygen, outperforming both higher-resolution simulations and the data-assimilative reanalysis in several cases where DA is known to be less effective because of sparse and intermittent observations. And these gains were achieved without assimilating ocean-colour chlorophyll or relying on increased spatial resolution. Additionally, both hybrid frameworks are designed to be transferable to other shelf-sea systems across the globe, as they are trained on globally available satellite-based productivity datasets and global experimental compilations of phytoplankton PI parameters.

2 Results

To help isolate the role of each experiment and benchmark in the results below, we summarise the simulations and reference systems used in this study in Table 1.

Table 1 Summary of model experiments and benchmark products used in this study.

ID	Experiment	Domain / grid	Res.	Primary production
LEGACY	Free-running (baseline	NWES (AMM7)	∼7 km	ERSEM (standard)
HYB-SF	Hybrid (ML-coupled)	NWES (AMM7)	∼7 km	ERSEM + ML scale factor
HYB-PI	Hybrid (ML-coupled)	NWES (AMM7)	∼7 km	ERSEM + ML PI parameters
REANALYSIS	Data-assimilative	NWES (AMM7)	∼7 km	ERSEM (standard) + DA
AMM15	Free-running (High-resolution)	NWES (AMM15)	∼1.5 km	ERSEM (standard)

2.1 Shelf-wide chlorophyll patterns in hybrid and process-based simulations

Chlorophyll serves as one of the primary metrics for marine ecosystem health largely because it is directly observable and closely linked to primary production. We therefore begin our analysis by comparing the results from the hybrid model simulations with those of legacy ERSEM against ocean-colour observations of chlorophyll from OC-CCI (Fig. 1).

Surface chlorophyll concentrations in the legacy simulation exhibited high root mean square error (RMSE) compared with those of OC-CCI with persistent errors in shelf and coastal waters during winter and spring (Fig. 1a,b). Over the shelf ($\leq$ 200 m), the legacy ERSEM simulation had the highest RMSE of 1.25, whereas the HYB-SF simulation reduced RMSE to 0.93 and the HYB-PI simulation to 1.16 (Table 2). The HYB-SF framework substantially decreased chlorophyll mismatches between model simulations and ocean-colour observations throughout the full study region. Improvements were especially observed during winter and spring (Fig. 1q,r) within the continental shelf for coastal areas, the entire North Sea, and the Norwegian coast. We observed shelf-wide improvements in the estimation of chlorophyll in the HYB-SF simulation during summer (Fig. 1s), but changes in autumn (Fig. 1t) remained largely neutral, with slightly increased RMSE in the shelf region.

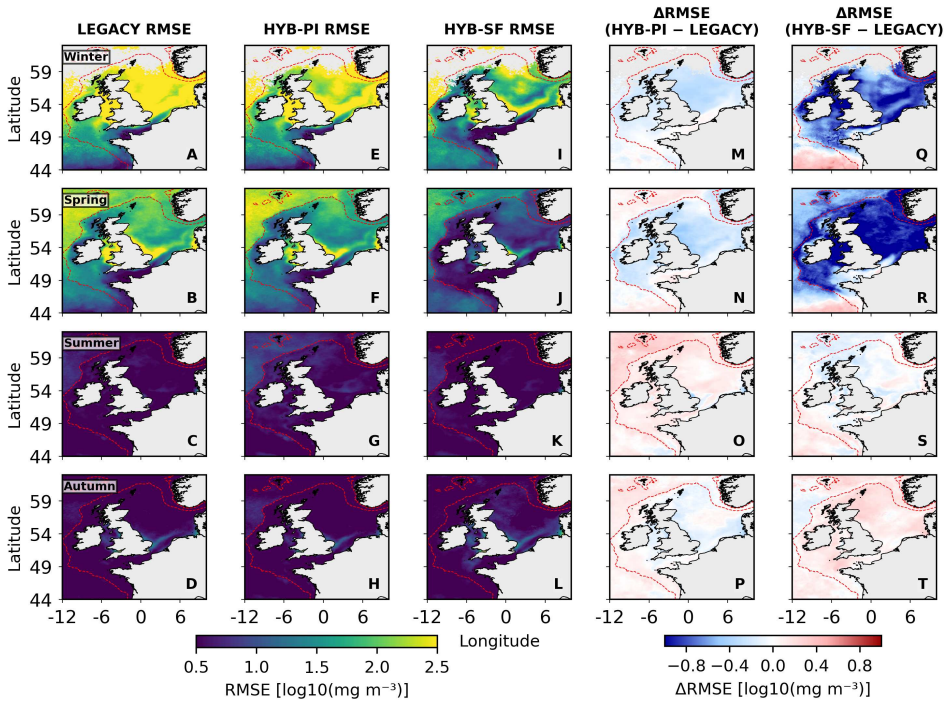

Fig. 1 Seasonal RMSE patterns (2017–2023 composite) for chlorophyll across the NW European Shelf, computed against OC–CCI satellite chlorophyll. Panels show RMSE of legacy ERSEM, HYB-PI, HYB-SF, and the seasonal RMSE differences (ΔRMSE) for Winter, Spring, Summer, and Autumn.

Region-averaged skill metrics (Table 2) showed similar results with the lowest RMSE in chlorophyll in the HYB-SF simulation. The results of the HYB-PI framework mostly showed RMSE values between the legacy ERSEM and HYB-SF simulations in all regions. One exception is in the English Channel, where the HYB-PI simulation showed the lowest RMSE values compared to chlorophyll concentrations from OC-CCI (Table 2). During winter, spring and autumn, improvements in the estimation of chlorophyll in the HYB-PI simulation were predominantly confined to the shelf region (Fig. 1m,n,p), consistent with the intended domain of physiological corrections, although a relatively high bias in chlorophyll existed during summer (Fig. 1o).

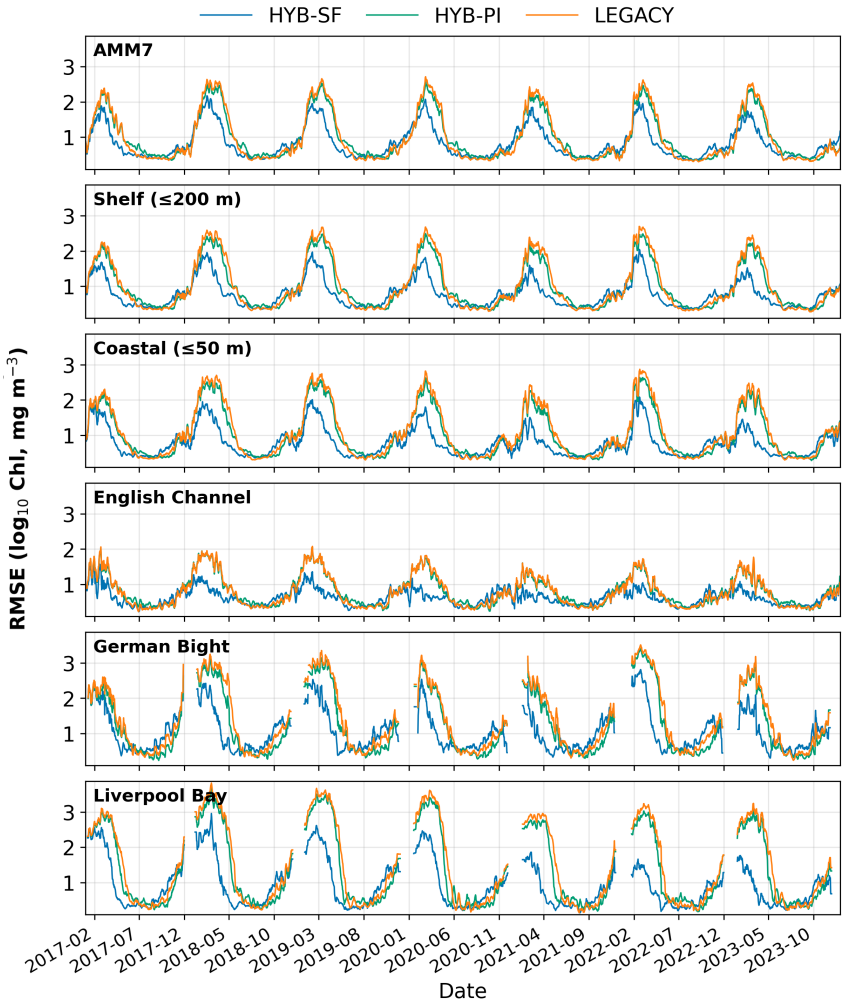

Fig. 2 Time-series of chlorophyll RMSE across key subregions of the NW European Shelf. Daily RMSE for legacy ERSEM, HYB-SF, and HYB-PI simulations over the shelf (≤200,m), Coastal (≤50,m), English Channel, German Bight, and Liverpool Bay.

Whilst basin-wide maps indicated where improvements to the estimation of chlorophyll occurred, time series analysis showed how the hybrid simulations stabilised the

Table 2 Region-wise bias and RMSE in $\log_{10}$ chlorophyll. Bold RMSE values indicate improvement relative to LEGACY.

Region	Run	Bias	RMSE
AMM7	LEGACY	0.13	1.23
	HYB-PI	1.11	**1.19**
	HYB-SF	0.46	**0.84**
Shelf (≤200 m)	LEGACY	−0.00	1.25
	HYB-PI	0.93	**1.16**
	HYB-SF	0.40	**0.77**
Coastal (≤50 m)	LEGACY	−0.72	1.34
	HYB-PI	0.20	**1.25**
	HYB-SF	−0.45	**0.83**
English Channel	LEGACY	−0.45	0.82
	HYB-PI	0.20	0.83
	HYB-SF	−0.54	**0.60**
German Bight	LEGACY	−2.13	1.62
	HYB-PI	−1.07	**1.49**
	HYB-SF	−1.70	**1.03**
Liverpool Bay	LEGACY	−1.09	1.80
	HYB-PI	−0.21	**1.68**
	HYB-SF	−0.91	**0.97**

seasonal cycle by reducing the amplitude of spurious peaks and dampening interannual variability in chlorophyll RMSE (Fig. 2). We estimated RMSE in chlorophyll across a set of regions, from the full AMM7 domain to several subdomains within the NWES. Results from the HYB-SF simulation consistently showed lower RMSEs in chlorophyll compared with OC-CCI across seasons and regions. The coastal areas exhibited the strongest improvement in model skill, with RMSE reduced from 1.80 in the legacy simulation to 0.97 and 1.68 in the HYB-SF and HYB-PI simulation, respectively (Table 2). During spring blooms, the legacy ERSEM simulation overshot OC-CCI chlorophyll, whereas the HYB-PI framework did not show a significant impact and mostly followed the results of the legacy simulation. Gaps in the German Bight and Liverpool Bay reflect satellite data gaps.

2.2 Spring bloom onset and associated nitrate dynamics

The seasonal growth cycle of phytoplankton, i.e., bloom phenology, is another important metric that can be used in monitoring and managing marine ecosystems. In the NWES, the seasonal cycle is typically characterised by a spring phytoplankton bloom, and we compared the onset of this bloom across all model simulations and that of satellite-based observations of chlorophyll (OC-CCI) for the latest simulation years 2022 and 2023 (Fig. 3a). We used the threshold cumulative distribution (TCUD) metric of Ferreira et al. (2014) [34] to estimate bloom onset, where onset timing is defined as the first day on which the cumulative chlorophyll reaches 15% of its seasonal total (based on gap-filled data and a 21-day running mean). The legacy simulation exhibited a systematically late spring bloom across much of the NWES domain, particularly in the Southern North Sea, the Celtic Sea, and the central basin (Fig. 3, top panel). This late bloom onset was reported previously in Butenschön et al. (2016) [20], where delayed onset in ERSEM relative to Western Channel Observatory time series and satellite observations was reported. Jardine et al. (2022) [35] also showed that ERSEM

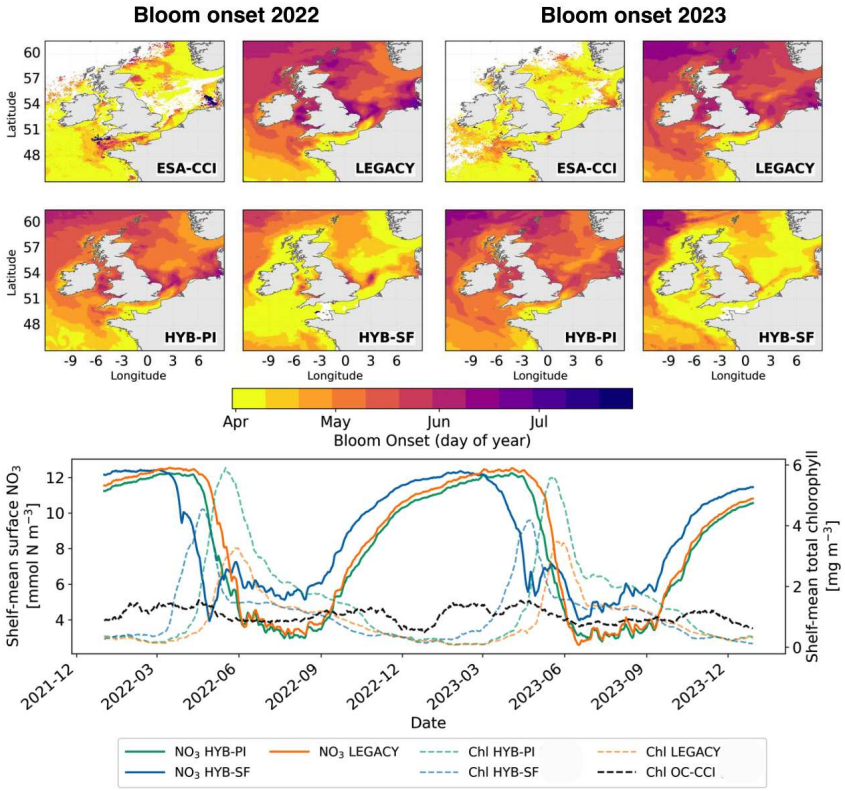

Fig. 3 Spring bloom onset timing and associated nitrate–chlorophyll dynamics across the NWES (2022–2023). Top panels: Spatial distribution of climatological spring bloom onset (day of year) derived from OC–CCI chlorophyll and simulated by legacy ERSEM, HYB-PI, and HYB-SF for 2022 and 2023. Earlier onset (yellow/orange) and later onset (purple/blue) are indicated by the colour scale. Hybrid configurations improved the spatial coherence and timing of bloom initiation, with HYB-SF showing the closest agreement with observations. **Bottom panel:** Shelf-mean surface nitrate (solid lines; mmol N m^{-3}) and total chlorophyll (dashed lines; mg m^{-3}) time series for the same period. Hybrid simulations modified both the timing and magnitude of spring bloom development and associated nutrient drawdown, signifying changes to internal production–nutrient coupling relative to the legacy ERSEM configuration.

can delay bloom onset by up to three weeks when light availability is underestimated. Additionally, Skákala et al. (2021, 2022) [12, 36] showed systematic late-bloom biases in biogeochemical reanalysis occurring particularly in stratified regions such as the central North Sea, together with a tendency to overshoot bloom magnitude.

HYB-SF simulation substantially improved bloom-onset timing by advancing it into the April–May window across most of the shelf in both years, producing similar results to OC-CCI and correcting the late-bloom bias in the legacy simulation. In 2022, the HYB-SF simulation captured relatively late bloom timing in the Southern North Sea and Irish Sea (end of May), in close agreement with OC-CCI, with similar improvements in 2023. The HYB-PI slightly improved onset timing relative to the legacy simulation, particularly capturing the later bloom along the eastern English Channel and the German Bight. The northward propagation of the bloom along the Atlantic boundary is more difficult to validate due to limited satellite coverage.

The improved bloom timing in the hybrid simulations was accompanied by distinct changes in nitrate dynamics. Time series analyses of chlorophyll and nitrate across the shelf demonstrate that the hybrid models reshaped ERSEM's primary production engine (Fig. 3, bottom panel). All simulations followed the classic chlorophyll-nutrient seasonal dynamics with winter recharge, spring drawdown, and summer minima of nutrients. HYB-SF showed an earlier bloom through dynamic scaling of primary production, resulting in an earlier chlorophyll peak and earlier nitrate uptake compared with the legacy simulation while retaining higher nitrate levels after the bloom. This showed that the scaling accelerated bloom onset without aggressively exhausting nutrients. The timing of the bloom onset in the HYB-PI simulation was between that of the HYB-SF and legacy simulation, with a higher chlorophyll maximum and faster depletion of nitrate. The legacy simulation showed a relatively delayed spring bloom with a lower amplitude in chlorophyll and less nutrient drawdown.

The bias in nitrate concentrations was evaluated using the NSBC level-2 climatology product (1960–2014) [28]. All model configurations exhibited a persistent positive nitrate bias across the shelf, consistent with previously reported behaviour of ERSEM-based systems [5, 37]. Relative to the climatology, the reanalysis showed the closest agreement, while the hybrid simulations did not systematically reduce shelf-wide nitrate biases (Supplementary Fig. S1).

In contrast, validation against ICES in situ nitrate observations showed modest improvements in the hybrid simulations relative to the legacy configuration, particularly with depth, whereas the reanalysis exhibited the largest near-surface bias and spread (Supplementary Fig. S4). Open-ocean validation using BGC-Argo profiles further indicated that the HYB-SF simulation produced a more realistic vertical nitrate structure and seasonal evolution, while HYB-PI tended to underpredict nitrate (Supplementary Fig. S3). Overall, nitrate improvements were limited compared with the gains achieved for chlorophyll, and are discussed further in the context of known uncertainties in nutrient forcing and riverine inputs.

2.3 Dissolved oxygen distributions across model configurations

We continue our assessment with dissolved oxygen, which is one of the important metrics that is often used in marine ecosystem management frameworks such as the European Union's Marine Strategy Framework Directive (EU MSFD) bottom-water oxygen criterion (D5C5) and the Water Framework Directive [38]. The seasonal bias in dissolved oxygen relative to the NSBC climatology in the legacy simulation showed that both hybrid runs restructured the surface oxygen distribution (Fig. 4).

The HYB-SF framework removed a widespread bias in surface dissolved oxygen of +40-90 mmol O_2 m^{-3} in summer across the domain (Fig. 4k) compared with the legacy model (Fig. 4c). We argue that the likeliest reason behind this is better coupling between primary production and respiration as hybrid frameworks adjusted net production rates in a way that reduced excess organic matter accumulation and associated over-oxygenation during summer. The HYB-PI simulation also reduced bias in dissolved oxygen concentrations (Fig. 4g), but to a much lesser extent than in the HYB-SF simulation and primarily in the central North Sea. Bias in dissolved oxygen remained essentially unchanged in autumn and winter across all simulations and was fairly aligned with the climatology (NSBC). During spring, the HYB-SF simulation showed a slight increase in bias in dissolved oxygen concentrations (Fig. 4j)

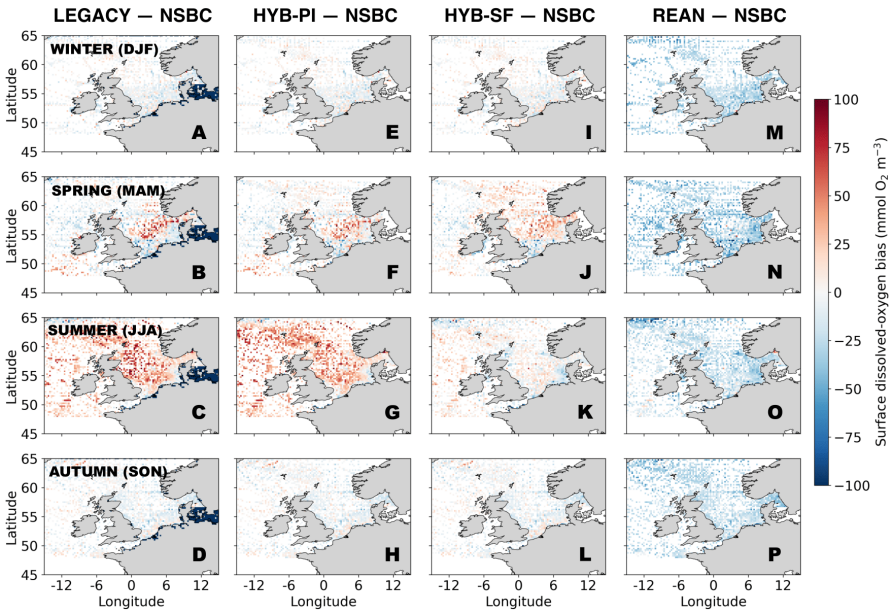

Fig. 4 Seasonal surface oxygen bias (2017–2023) for legacy ERSEM, hybrid simulations and reanalysis against NSBC Level-2 climatology Summer showed the strongest signal, where both hybrid runs reduced large positive summer and year-round negative surface oxygen bias present in legacy and reanalysis, respectively, across the whole domain.

compared with the legacy simulation (Fig. 4b) in the North Sea region, whereas the HYB-PI simulation (Fig. 4f) stayed closest to the climatology (NSBC), with a slight overestimation in the central North Sea.

Comparison of the NSBC with the reanalysis which is considered the operational benchmark for regional marine ecosystem assessments [39, 40] and is used in daily forecasting services, showed a strong negative bias in dissolved oxygen concentrations year-round (Fig. 4m-p), often between -30 and -50 mmol O_2 m^{-3} (as also reported in the product Quality Information Document [13]). The HYB-SF simulation aligned with the NSBC climatology better than the HYB-PI simulation and reanalysis, reducing the winter–autumn mismatch and suppressing summer excess in dissolved oxygen between +30 and +60 mmol O_2 m^{-3} (Fig. i-l). However, when compared with the reanalysis, improvements in the HYB-PI simulation were localised (Fig. e-h): The overall negative bias was largely removed, but a localised surplus remained during summer. Nevertheless, both hybrid models performed noticeably better than the reanalysis, even though dissolved oxygen was never explicitly targeted during the training or prediction phases of either hybrid model.

Additionally, validation with in situ oxygen data from ICES confirmed that the HYB-SF framework delivered the strongest overall skill in estimating dissolved oxygen concentrations, with the smallest bias (5.51 mmol O_2 m^{-3}), the lowest RMSE (35.20 mmol O_2 m^{-3}), and the highest correlation (0.48) (see Supplementary Fig. S4). The HYB-PI framework reduced over-oxygenation as seen in the legacy simulation, but exhibited a small number of low-oxygen outliers, while dissolved oxygen levels were consistently underestimated in the reanalysis. Depth-resolved diagnostics showed that both hybrid simulations exhibited narrower errors from the surface to deeper layers.

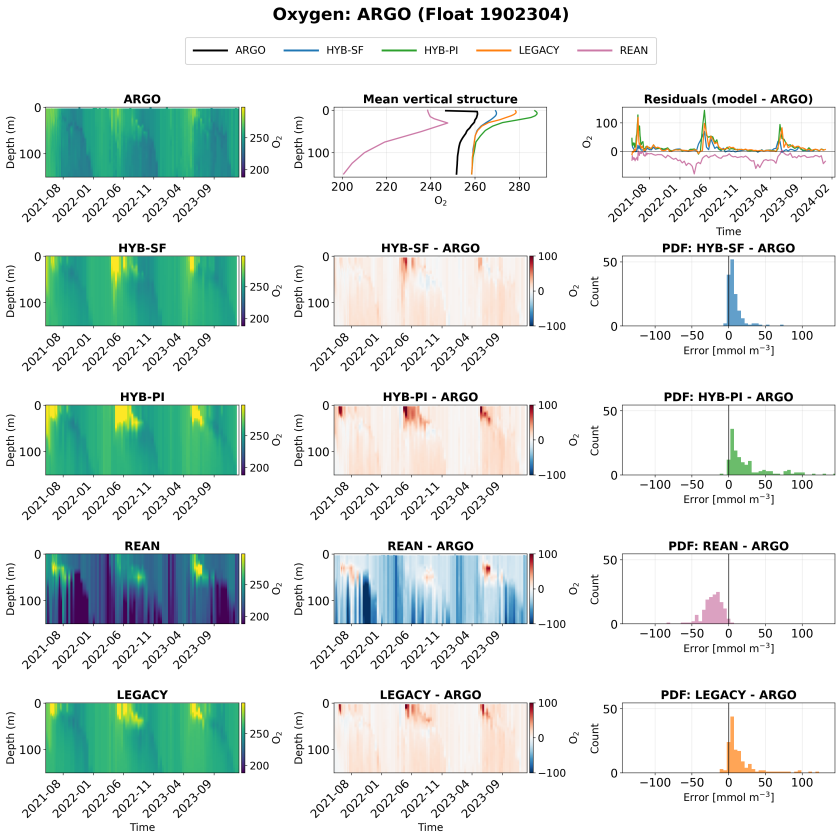

Fig. 5 Validation of simulated dissolved oxygen against a representative BGC-Argo float (ID 1902304; 48.87°N, 14.85°W). Panels compare observed BGC-Argo dissolved oxygen profiles with simulations from legacy ERSEM, HYB-SF, HYB-PI, and the reanalysis. HYB-SF removed the systematic negative bias present in the reanalysis and reproduced the observed spatio-temporal (Hovmöller) structure, with minor overestimation near the surface. Residual time series and vertical profiles showed that HYB-SF exhibited the narrowest error PDF (probability density functions) distribution centred around zero, whereas the reanalysis remained skewed toward negative errors. HYB-PI reduced much of the reanalysis bias but retained a surface-intensified positive bias following the bloom.

To assess whether corrections introduced within the shelf-sea production engine propagated coherently beyond the shelf and through the water column, we further evaluated the hybrid systems against independent oxygen profiles from BGC-Argo floats in the adjacent open ocean. We compared our hybrid simulation with BGC-Argo oxygen profiles available within the domain and found consistent behaviour across multiple floats, with one representative example analysed here. This comparison further supported the above results (Fig. 5). The HYB-SF simulation showed the greatest match with the observed vertical oxygen profiles over the years, whilst the reanalysis consistently underestimated dissolved oxygen levels. The residual and mean dissolved oxygen profiles confirmed that the HYB-SF simulation showed a narrower spread and the most realistic vertical oxygen distribution, while the HYB-PI simulation retained a surface-biased signal during the post-bloom period. Together, these results showed

that hybrid corrections noticeably improved model skill to estimate dissolved oxygen from the surface to deeper layers.

2.4 Comparison of hybrid chlorophyll simulations with biogeochemical reanalysis

Here we continue with a comparison of chlorophyll estimated from hybrid simulations against CMEMS ocean-colour level-4 biogeochemical observational data products [41], which were also used for validation of the reanalysis. We treat this comparison separately because it addresses a fundamentally different question from model–observation skill alone: how ecosystem models perform when DA is absent or ineffective. The data assimilative CMEMS NWES reanalysis system relies on the continuous availability of observation streams that constrain surface PFT (phytoplankton functional type)-specific chlorophyll distributions [42], sea surface temperature, and subsurface temperature–salinity structure [13]. However, in many shelf-sea regions and seasons, ocean-colour observations are intermittent or unavailable due to cloud cover, high turbidity, or low solar angles, leaving reanalysis systems effectively unguided, resulting in unrealistically low winter chlorophyll as reported in the reanalysis [13]. A similar study by Ciavatta et al. (2016) [43], done in the same domain, showed that the biogeochemical model-data assimilation system consistently underestimates chlorophyll in coastal zones such as the southern North Sea and the German Bight. Skákala et al. 2018 [5] reported that assimilating ocean-colour observations improves large-scale patterns but frequently suffers from significant biases. Therefore, evaluating the hybrid simulations against the identical observational reference used by the reanalysis validation provides a direct and fair assessment of whether embedding data-informed corrections incorporated in the model dynamics can improve forecast skill, particularly under conditions where observational constraints are weak. This distinction is critical for assessing the effectiveness of hybrid models as standalone predictive modelling systems and as potential candidates for future assimilation frameworks. In addition, using an independent ocean-colour product for this comparison provides a stringent test of the scientific robustness and generalisability of the hybrid framework beyond the datasets used to inform its development.

The RMSE for each model simulation and the reanalysis was determined using the CMEMS ocean-colour product and then represented by Δ RMSE: the difference between chlorophyll RMSE in legacy, HYB-PI and HYB-SF simulations and the RMSE of reanalysis for 2017–2023 composite and for the same that of the latest simulation year, i.e., 2023 (Fig. 6). We noticed that both hybrid frameworks improved chlorophyll accuracy (against CMEMS ocean-colour data) at the ocean surface throughout most of the year compared with the legacy simulation (2017–2023). These improvements happened mostly in winter, spring, and summer, with a slight change in autumn. During the spring bloom season, the HYB-SF simulation showed the highest reduction in RMSE for the full time period (Fig. 6j) and for 2023 (Fig. 6n) compared to the legacy simulation (Fig. 6b), especially in areas of the Western English Channel, Celtic Seas, and the Irish Sea, where shifts towards neutral (i.e., RMSE = 0) were observed, meaning that the hybrid model is equal to the reanalysis. We observed substantial improvement in winter during the last simulation year, 2023 (Fig. 6m). During this period, the HYB-SF simulation showed shelf-wide negative RMSE difference going as low as -2 $\log_{10}$(Chl), corresponding to reductions in multiplicative error in chlorophyll

concentration of up to two orders of magnitude. This demonstrates the ability of the hybrid model to bring simulated chlorophyll concentrations into close agreement with the observation, without direct assimilation of ocean-colour data during the model integration. Prominent areas of improvement were observed, especially in UK coastal waters, including the English Channel, except in some parts of the North Sea. Similar model skill in the HYB-SF simulations was observed in summer (but not as high as in winter), with notably better surface chlorophyll distribution than the reanalysis, particularly in the Southern North Sea and in the English Channel during 2023 (Fig. 6k,o). The HYB-PI simulation showed slight improvements compared with the legacy simulation, lying mostly between the HYB-SF and legacy ERSEM simulations (Fig. e-h), with the strongest improvements confined to the English Channel and the German Bight.

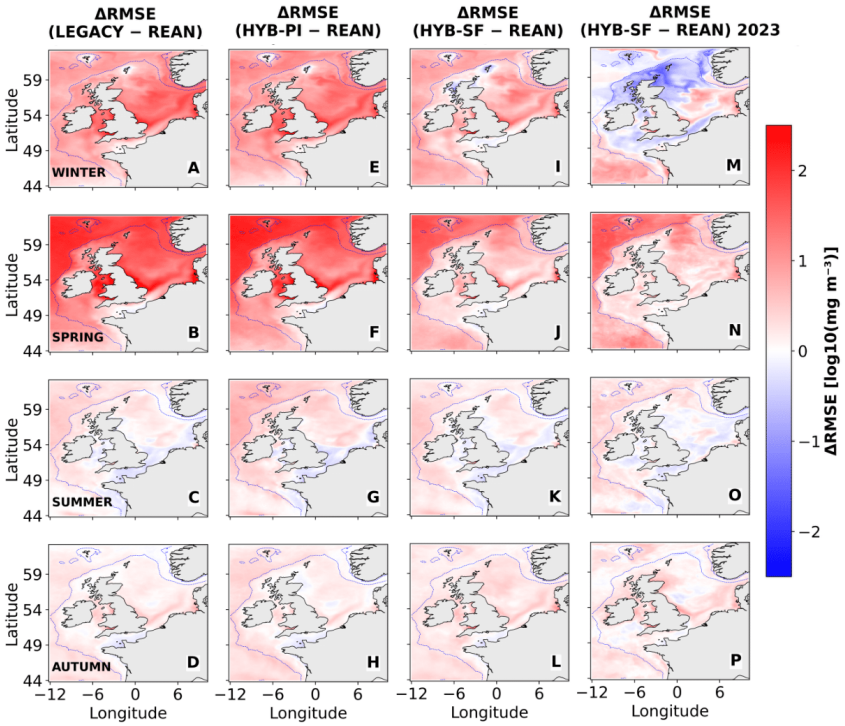

Fig. 6 Seasonal ΔRMSE (model − reanalysis) for chlorophyll (2017-2023 composite and the latest simulation year, 2023). Across all seasons, both hybrid systems reduced the large shelf-wide RMSE seen in legacy ERSEM, with HYB-SF showing the greatest improvements when compared to reanalysis, especially during the 2023 summer and winter, where a considerable area of the shelf-sea shifted towards neutral or negative ΔRMSE, indicating an equal or stronger agreement with observed chlorophyll than the reanalysis.

Time series analysis of RMSE in chlorophyll showed results that are consistent with the spatial maps. The HYB-SF simulation maintained the lowest RMSE in chlorophyll of the legacy and hybrid simulations throughout all regions throughout the simulation period, staying closest to the RMSE in reanalysis and exhibiting similar and better skill than the reanalysis during 2023 (Fig. 7, Supplementary Table S2). The HYB-PI

simulation showed RMSE in between the HYB-SF and legacy simulations, showing improvements in timing and amplitude of seasonal peaks in chlorophyll. An interesting observation was the gradual decrease in RMSE for chlorophyll in the HYB-SF simulation across most regions over time. This may be expected since the hybrid simulation starts on January 1, 2017 (same initial conditions as in legacy simulation) and the model re-equilibrated the ERSEM nutrient and carbon structures after completing one seasonal cycle, i.e., the physics-AI-biology coupling needed longer simulations to settle into its new dynamical balance, and it is the subsequent years where the true behaviour of the system emerged.

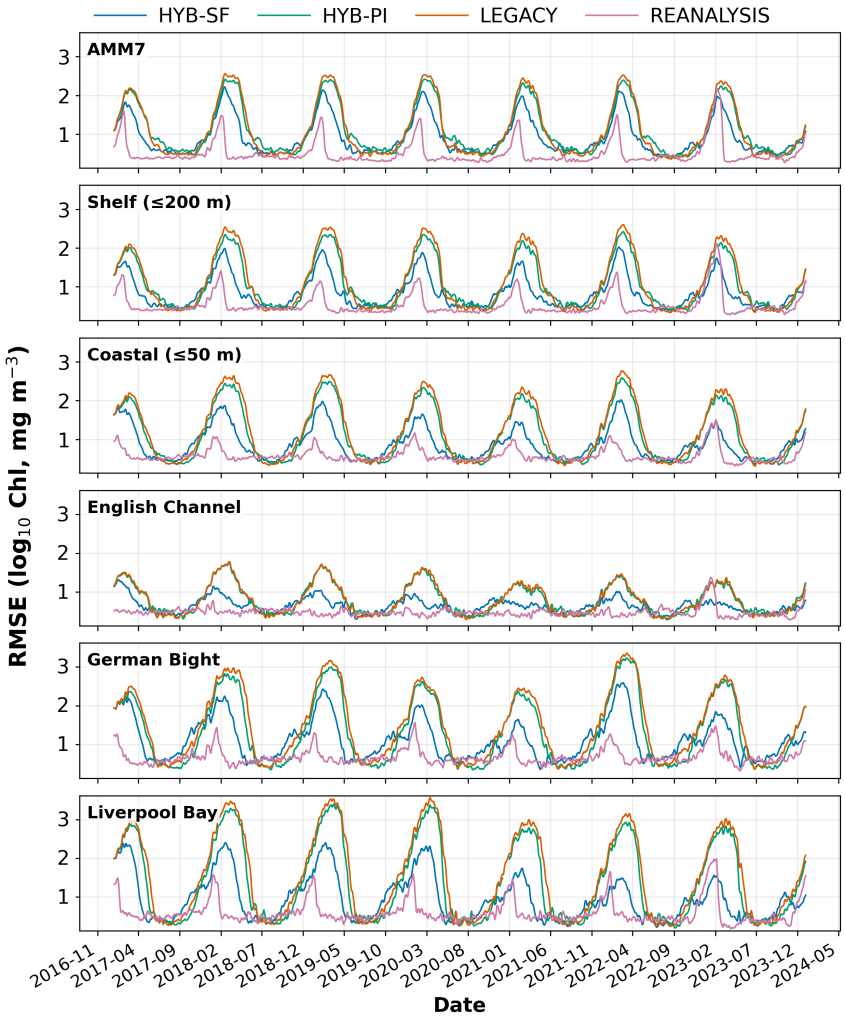

Fig. 7 Regional chlorophyll RMSE time series against CMEMS ocean-colour product. Daily RMSE is shown for the AMM7 domain, shelf (≤200 m), coastal waters (≤50 m), the English Channel, the German Bight and the Liverpool Bay, comparing legacy ERSEM, HYB-SF, HYB-PI and the reanalysis. HYB-SF stayed closest to the reanalysis and showed the best skill scores during the most recent year 2023, with HYB-PI lying between HYB-SF and the legacy ERSEM.

We compared our hybrid simulation with BGC-Argo chlorophyll profiles available within the domain and found consistent behaviour across multiple floats, with one representative example analysed here. Supplementary Fig. S2 shows that the HYB-SF framework removed the subsurface overestimation as observed in the reanalysis, representing the post-bloom subsurface structure most realistically. The residuals also showed a tighter distribution, clustered around zero. Yet, the HYB-PI simulation overshot chlorophyll and showed a broadest error spread, underperforming at the location of the BGC-Argo float.

2.5 Comparison of hybrid chlorophyll simulations with the high-resolution AMM15 model

We further compared RMSEs in the surface chlorophyll distribution from the two hybrid simulations with a free-running high-resolution AMM15 simulation (1.5 km; Partridge et al., 2025 [33]), currently used by the UK Met Office for operational forecasting [44], after regridding the AMM15 model output onto the AMM7 domain for a consistent comparison, using OC-CCI chlorophyll [30] as the reference (Fig. 8).

The HYB-SF simulation performed better than AMM15 right across the NWES domain during the bloom months, with a clear drop in RMSE in spring (Fig. 8f). The HYB-PI simulation also showed improved chlorophyll simulation over AMM15 during spring (Fig. 8b), though the improvements were more localised around UK coastal and shelf waters, which would be expected from a physiology-informed hybrid model. We found that during this season, HYB-PI simulation showed slightly higher RMSE than AMM15 in the open ocean beyond the shelf, which may be expected since the model was neither trained nor actively predicting PI parameters outside the shelf domain. The HYB-SF simulation showed lower RMSE in chlorophyll in winter along coastal margins (Fig. 8e), while the HYB-PI simulation mostly aligned with AMM15 (Fig. 8a). Although during winter, observational coverage was limited. Both hybrid frameworks performed similarly to AMM15 in summer (Fig. 8c,g) and autumn (Fig. 8d,h), although we noticed slightly higher positive biases in these seasons. Analysis of the time series (see Supplementary Table S1) confirmed these results, with the HYB-SF framework performing best across seasons and regions. The HYB-PI framework further showed better model skill in estimating chlorophyll compared with AMM15 and even exceeded it during the spring bloom (see Supplementary Table S1).

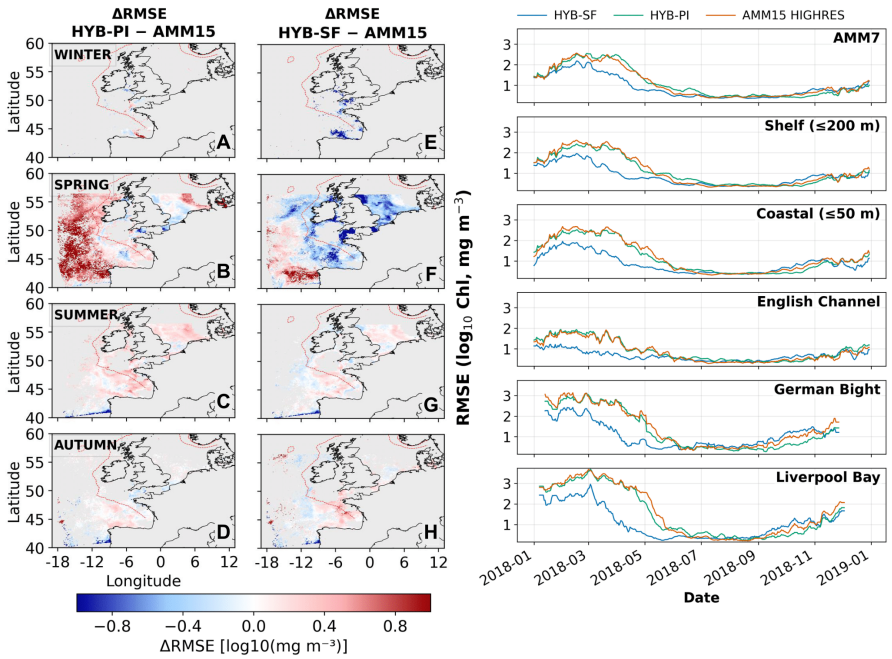

Fig. 8 Seasonal chlorophyll RMSE comparison against AMM15. The left two columns show seasonal ΔRMSE for HYB-PI, HYB-SF with AMM15. Blue indicates improvement and red indicates degradation with respect to AMM15. HYB-SF showed widespread spring improvement (panel D) across the shelf, while HYB-PI showed local gains around the English Channel and coastal zones (panel C), but overestimated in off-shelf. The right panel shows time-series RMSE for surface chlorophyll across several spatial domains. HYB-SF consistently outperformed AMM15 across the full AMM7, shelf, and coastal regions. HYB-PI exhibited similar performance to AMM15 and some selective improvements during the bloom season.

3 Discussion

Both hybrid models fundamentally adjusted the process-based model's native representation of primary production. The satellite-trained version (HYB-SF) acts as an online bias-corrector, improving chlorophyll and oxygen distributions throughout a complex shelf-sea environment. On the other side, the physiology-informed variant (HYB-PI) focuses on the phytoplankton's light-response by adjusting the PI parameters, yielding better results in specific regions such as the English Channel and the German Bight, precisely where local photophysiology governs bloom behaviour. In comparison, the HYB-SF simulation evidently outperforms the HYB-PI simulation in both magnitude and spatial extent for the analysed variables (i.e., chlorophyll, dissolved oxygen and nitrate) in our test, owing to its direct, shelf-wide correction of net primary production. Nevertheless, HYB-PI consistently brings the simulation closer to observations in niche regions where the PI curve training is most representative, largely representing the shallow-water experimental datasets on which it was trained. This outcome is scientifically expected as it accentuates the mechanistic nature of this particular approach. HYB-PI modifies phytoplankton photophysiology but is constrained by the available experimental knowledge. Further improvements in HYB-PI

can be expected through expansion of the observational training dataset to better represent variability across depths, seasons, phytoplankton communities, and additional growth-limiting factors, in line with a recent perspective emphasising closer integration of empirical plankton knowledge to improve the reliability and utility of ecosystem projections [45].

There is one prominent area where both hybrid models can be further refined. An important shortcoming lies in the nutrient simulation. Despite improved chlorophyll and oxygen skill, nitrate biases may persist due to uncertainties in riverine nutrient inputs, which vary across space and season and can only be addressed through nutrient data assimilation. Future work could address this issue by relaxing or assimilating machine-learned nutrient data into the hybrid systems, following the work by Banerjee et al., 2025 [46, 47]. Nevertheless, a key aspect of this work is that all improvements are achieved without assimilating nutrient data; by modifying model productivity rates and adjusting phytoplankton's photophysiological response alone, whilst the system remains fully mass-conservative.

From an operational point of view, our hybrid frameworks represent a promising framework of efficient and skilful forecasting systems. They match or exceed the accuracy of data-assimilative reanalysis and high-resolution regional models in several challenging areas and seasons, even when running at coarser resolutions without continuous DA. This demonstrates the scientific validity of integrating empirical knowledge directly into a process-based model's core dynamics. Our results indicate two important findings: (1) increasing spatial resolution alone can yield incremental improvements, but persistent biogeochemical biases ultimately originate from limitations in the underlying process representations, and (2) amalgamation of empirical knowledge with process-based models emerges as a promising alternative, particularly where DA is not viable, either because observations are intermittent or fundamentally unreliable. Additionally, the neural network components are compatible with future GPU (Graphics Processing Unit)-accelerated implementations for faster simulations, making our hybrid framework suitable for operational adaptation, although such applications were not explored here. Furthermore, owing to its parallel architecture and AI/ML transferability across shelf seas, the framework delivers a clear pathway toward worldwide real-time operational applications in future works.

Technologically, our hybrid framework stands apart from standard machine-learning approaches in environmental sciences [48–51]. While Physics-Informed Neural Networks (PINNs) embed physical constraints into AI models, we invert this logic through "Neural-Network-Informed Physics" (NNIP). In NNIP, established process-based equations remain the primary drivers, with AI providing physics-constrained, data-informed adjustments where empirical knowledge is limited. This ensures physical and biological conservation laws are strictly preserved, making the model stable and interpretable. While related ideas have emerged in physical oceanography [52], they have not yet been formalised within coupled biogeochemical forecasting systems.

Several studies have reported climate projections with warming-driven deoxygenation conditions in temperate shelf seas (due to temperature-driven solubility loss, stronger stratification, and circulation changes) [53, 54]. In this context, notably, our simulation period, 2017–2023, lies well beyond the AI training period (2002–2015 for HYB-SF and 1977–2013 for HYB-PI), yet both hybrid systems remain stable and continue to improve oxygen prediction. This persistence of skill beyond the training

period highlights the potential of hybrid frameworks to support future climate projections of ecosystem productivity and oxygen dynamics when integrated with Earth System Models.

Beyond technical results, our work addresses the wider challenge of developing sustainable ecosystem modelling frameworks for shelf-sea ecosystems that achieve significantly improved prediction skill without increasing computational cost. The interpretable, domain-constrained AI components of our hybrid framework exemplify the ethical use of artificial intelligence in line with emerging environmental AI principles that emphasise transparency and reliability in environmental applications, including the UK's Net Zero Strategy and related international AI governance frameworks [55–57]. Additionally, improved ecosystem forecasts from our hybrid framework have clear potential to support marine environmental assessment and reporting (e.g., the Marine Strategy Framework Directive, MSFD) and may inform wider marine policy objectives, including fisheries sustainability under the UK Fisheries Act 2020 [58], habitat protection under the UK Marine Strategy (UKMS), and international commitments for example the United Nations Sustainable Development Goal 14 (UN-SDG14: Life Below Water) [59]. Moreover, our hybrid framework's low cost and energy use also lowers the barrier to adoption, making it accessible for agencies without exascale high-performance computing infrastructure. This aligns with the global shift toward more responsible and efficient climate models and agrees with several government policies across the world, where there is emerging evidence showing recent developments on data-intensive workflows, including high-resolution modelling and assimilation, are contributing to rising electricity demand [60].

We demonstrated that integrating ML adjustments directly into a process-based model during simulation improves prediction skill without increasing complexity. Using AI to adjust process rates and model parameters provides greater flexibility than static parameterisations, which opens opportunities to streamline complex ecosystem models while maintaining predictive skill and reducing computational cost. While tested here in a temperate shelf-sea, our paradigm offers a scalable foundation for next-generation ecosystem prediction across regional and global climate frameworks.

4 Methods

4.1 Process-based modelling framework

We use the NEMO ocean engine [61] as the hydrodynamic component, coupled online through FABM [62] to ERSEM for lower-trophic ecosystem dynamics. NEMO provides ocean-physical data such as temperature, mixing, and advection. FABM handles the fluxes and state exchanges, while ERSEM calculates the biogeochemical terms such as phytoplankton growth, nutrients, and oxygen. Our NWES setup uses the AMM7 grid with about 7 km resolution. This is the same grid used by CMEMS and the UK Met Office for this region.

4.1.1 NEMO Physics

The physical component, NEMO, is a finite-difference, hydrostatic ocean general circulation model that solves the primitive equations governing momentum, temperature, and salinity. The NEMO configuration used in this study is almost identical to Skákala et al. 2020 [63] and Ford et al., 2018 [64]. A CO6 version of NEMO is used in this

study, which is based on NEMOv3.6, an updated version of the CO5 configuration as depicted in detail by [65]. The spatial resolution of the model is approximately 7 km on the Atlantic Margin Model (AMM7) domain. The model uses a terrain-following vertical coordinate system with 51 levels. This setup improves the representation of stratification and mixing. It also makes the benthic-pelagic exchange more realistic across different depths. This is particularly important when coupling the physics with biogeochemical models. In our experiments, the lateral boundary conditions for physical variables at the Atlantic boundary were obtained from the North Atlantic deep ocean model [66] and Baltic boundary conditions from the Copernicus operational Baltic Sea model [67]. The river discharge data for NEMO were extracted from the UK Met Office Unified Model global numerical weather prediction system [44].

4.1.2 ERSEM Biogeochemistry

ERSEM, the biogeochemical model, represents the lower trophic levels of marine ecosystems with the capability of resolving pelagic plankton communities and benthic fauna and driving nutrient and carbon cycling in coastal and shelf seas [68]. ERSEM also possess the capability to simulate plankton dynamics resolved into four PFTs largely classified by size [19], i.e., picophytoplankton, nanophytoplankton, diatoms and dinoflagellates. Each PFT's biomass is represented in multiple biogeochemical currencies, i.e., chlorophyll, carbon, nitrogen and phosphorus, with diatoms additionally represented by silicate. ERSEM uses variable stoichiometry, i.e., the ratios of carbon, nitrogen, and phosphorus change dynamically depending on the environment (light availability, nutrients, etc.) [69]. The model predators include three main zooplankton groups, such as mesozooplankton, microzooplankton, and heterotrophic nanoflagellates [20], where decomposed organic matter is handled by a single group of heterotrophic bacteria that recycles nutrients back into the system. Apart from simulating the living organism, ERSEM also tracks nutrients (nitrate, phosphate, silicate, ammonium, carbon), as well as dissolved oxygen, gaseous substances, and water. ERSEM further includes the carbonate system, which can simulate CO_2 and its interactions with the atmosphere, a key component for ocean acidification studies [70].

4.1.3 FABM coupling and Python embedding

FABM [62] is a generic coupling layer that provides stable APIs (Application Programming Interfaces) to link physical models (e.g., NEMO) with any number of biogeochemical components (e.g., ERSEM). Traditionally, these biogeochemical components were coded in Fortran, but recent releases of FABM (v3 and up) optionally embed the Python interpreter to access biogeochemical components written in Python. Here, we exploit this new functionality to combine ERSEM's existing Fortran-based components with a custom Python-based machine learning model. The FABM layer allows both types of components to exchange information. Only minimal adjustments to the ERSEM code were needed to obtain selected process parameters from our ML component. The physical model (NEMO) links to the FABM library as usual and remains unaware of the Python interpreter and any ML libraries running underneath.

4.2 Hybrid system architecture

By adding two machine learning modules into ERSEM, we created two separate hybrid versions, which we simulated independently and compared. It is to be noted that the AI modules are neither external bias correction nor post-processing routines; they are fully integrated within the ecosystem model and run as one of its components that interact with the biogeochemical routines at every timestep, modifying the core productivity dynamics whilst preserving the underlying physics, i.e., mass balance and stoichiometry ratios. In other words, a numerical model, i.e., ERSEM, does not "follow" a machine learning algorithm, but the machine learning informs ERSEM at the exact point in time and space where the process formulation is known to struggle.

4.2.1 Machine-learned primary productivity scale-factor hybrid (HYB-SF)

In the first hybrid setup (HYB–SF), we corrected baseline process-based model's primary production with a scale factor using a machine learning model trained against the satellite-derived primary productivity, estimated using chlorophyll-a concentrations from the Ocean Colour Climate Change Initiative (OC-CCI version 6 [30]; Sathyendranath et al. 2019 [21]), Photosynthetically Active Radiation from National Aeronautics and Space Administration (NASA) and seasonal climatologies of photosynthesis-irradiance and chlorophyll-profile parameters that were assigned per Longhurst province [71] as described in Kulk et al. [22]. Uncertainty in satellite-based primary production was estimated using a Monte Carlo simulation to propagate errors in chlorophyll and PI parameters [22]. We mapped this dataset (4 km resolution) from March 2000 to December 2015 onto the AMM7 grid and trained the model on the logarithm of the satellite-to-model productivity ratio, which quantifies the systematic bias of the baseline model relative to satellite estimates.

The feature set was deliberately made compact, shelf-focused, and runtime-accessible via ERSEM (see Supplementary Table S5). It includes sea surface temperature (SST) from European Space Agency (ESA) AVHRR (Advanced Very High Resolution Radiometer) L2P v3.0 [72], MODIS-Terra monthly PAR (Photosynthetically Active Radiation) [73], 10 m wind from ERA5 [74], Sea Surface Salinity (SSS) from Atlantic- European North West Shelf- Ocean Physics Reanalysis NWSHELF_MULTIYEAR_PHY_004_009 [75], longitude, latitude, bathymetry, astronomical daylength, PAR × daylength, wind-speed squared, log(1 + depth), SST × PAR, and month encoding (sine and cosine).

Daylength was estimated analytically following Forsythe et al. 1995 [76]:

$$D = \frac{24}{\pi}\,\omega, \qquad \omega = \arccos[-\tan(\phi)\,\tan(\delta)]\,,$$

$$\delta = 0.409\,\sin\!\left(\frac{2\pi\,(t-80)}{365}\right),$$

where ϕ is latitude and t denotes the day of year.

The algorithm was implemented both offline during AI/ML training and online within ERSEM via FABM–Python without additional input-output (I/O) operations. The SST–PAR product acts as a proxy to the metabolic–radiative synergy. We used

depth as $\log(1+H)$ to ensure the bathymetric span that would distinguish shallow-shelf biogeochemistry from the deeper open ocean.

For our training data, we kept only the points from the continental shelf (depth ≤ 200 m). We also made sure that primary productivity from both sources was positive and finite. Finally, we clipped the ratios to a range between 0.05 and 6 to remove any outliers before training. To improve data quality, satellite-derived primary productivity estimates with higher uncertainty were down-weighted. This makes the training more reliable. The dataset spans from March 2000 to December 2015. We used 2000–2012 for training, 2013–2014 for validation, and 2015 for the test phase.

We used `HistGradientBoostingRegressor` as our best performing AI/ML model for its balance of flexibility, speed, and skill, achieving $R^2 = 0.80$ on validation and $R^2 = 0.83$ on test (see Supplementary Table S7 and Supplementary Fig S9). A SHAP (SHapley Additive exPlanations) analysis was performed to assess the relative contribution of each predictor to the learned scale factor, confirming that seasonal harmonics, daylength, bathymetry, and radiative–thermal interactions dominate the model behaviour (see Supplementary Fig. S10). The model Hyperparameters were tuned via Optuna [77] in log-space, and additionally, two optional weighting schemes were tested: (1) linear-ratio tail weighting and (2) weighting with the uncertainty associated with the satellite-derived primary productivity model, used in the loss function during training. The final trained model and scalers were combined into a single portable bundle for use in the ERSEM simulation.

During ERSEM's runtime prediction, the FABM–Python wrapper reads the features, i.e., SST, PAR, depth, wind, location, and day-of-year at each horizontal grid cell per timestep and the same predicted feature values are then used throughout the water column; however, its effective influence is naturally confined to the euphotic layer through ERSEM's light-dependent growth formulation and vertical attenuation, rendering corrections negligible at depth. During each integration timestep, ERSEM reconstructs the feature vector and the coupled ML model predicts the log-ratio, and converts it back to linear scale. Same scale factors are applied across all PFTs.

We used three physical safeguards before using scale factors in process-based model's online prediction: (1) conditions such as low light, deep ocean, non-finite input make the scale factor to 1 (meaning no correction); (2) strong deviations are softly pulled toward a factor 1 using a pair of sigmoids; (3) any failure returns a neutral value, ensuring native ERSEM behaviour is retained under uncertainty. By using these safeguards, we keep the model stable and ensure that the corrections are conservative. This way, the hybrid system stays within a scientifically acceptable range.

4.2.2 Machine-learned PI parameters hybrid (HYB–PI)

For the HYB-PI model, we replaced the standard photosynthesis formulas in ERSEM. Now, the model predicts α^B and P_m^B dynamically using an ML emulator. This emulator was trained on data from Bouman et al. (2018). α^B controls light sensitivity and P_m^B sets the ceiling for growth. This way, the model dynamically adapts to light and temperature during integration.

To train the model, we selected shelf data (depth $\leq$ 200,m, $\alpha \leq 0.12$), which provided $N \approx 2000$ samples. We split the data 80/20 for training and validation and used Optuna [77] for optimisation. On the validation set, the R^2 scores were 0.48 for α^B and 0.56 for P_m^B. The 5-fold cross-validation results were 0.42 ± 0.03 and 0.56 ± 0.02 (detailed in Supplementary Table S3, Supplementary Fig. S7 and Fig. S8)

During the simulation, the numerical model (ERSEM) calls the emulator once per grid column and timestep. It uses features such as SST, PAR, wind, and location, as in the HYB-SF setup (see Supplementary Table S3). To stay within safe limits, we only use predictions for depths ≤ 200 m, PAR ≥ 5 W m^{-2}, and daylength ≥ 2 h. If inputs are invalid, the model returns zero and keeps the original ERSEM behaviour.

The emulator calculates vertical profiles for α^B and P_m^B. During training, we capped α at 0.12. Notably, we only apply the ML-predicted parameters where chlorophyll is present (ChlCpp > 0) and the results are finite. For the unit conversions, we followed standard radiometric mappings:

$$\alpha_{\mathrm{ERSEM}} = \alpha_{\mathrm{Bouman}} \times 24 \times 4.57, \quad \mathrm{sum}_{\mathrm{loc}} = P^B_{m,\mathrm{day}} \times \mathrm{ChlCpp}.$$

Here, α_{Bouman} and $P^B_{m,\mathrm{day}}$ denote the PI slope and daily maximum chlorophyll-specific photosynthetic rate predicted by the emulator following Bouman et al. (2018), respectively. These quantities are converted to the corresponding ERSEM parameters, α_{ERSEM} and $\mathrm{sum}_{\mathrm{loc}}$, which represent the light-limited growth coefficient and the local maximum photosynthetic rate used internally by ERSEM. To ensure physiological and numerical stability, we enforced strict bounds. We discarded the corrections where predicted values are non-finite, negative, or exceed $2\,\alpha$ or $\min(2.5\,\mathrm{sum}, 5\,\mathrm{d}^{-1})$ ensuring the ML-adjusted maximum productivity cannot exceed 2.5× native ERSEM or the $5\,\mathrm{d}^{-1}$ ceiling. Outside these prescribed thresholds, the numerical model defaults to its uncorrected PI parameters whilst keeping HYB–PI fully constrained within its trained environmental regime and yet able to respond dynamically in space and time.

4.3 Validation datasets and evaluation metrices

We validated our simulations using:

- Satellite chlorophyll, extracted from the ESA Ocean Colour Climate Change Initiative merged Level-3 daily product (version 6.0, 1 km) [30].
- CMEMS ocean-colour Level-4 biogeochemical observation [41]
- In situ BGC-Argo float profiles (chlorophyll, nitrate, oxygen) [78]
- In situ oxygen and nitrate profiles from International Council for the Exploration of the Sea (ICES) [32].
- NSBC Level-2 climatology [28].
- CMEMS Atlantic–European North West Shelf-Ocean Biogeochemistry Reanalysis `NWSHELF_MULTIYEAR_PHY_004_009` [13] to benchmark hybrid simulations.
- NEMO-ERSEM high-resolution model simulations from high-resolution 1.5 km Atlantic Margin Model (AMM15) configuration from Patridge et al. (2025) [33] to further benchmark hybrid simulations.

Spatial RMSE in $\log_{10}$ space (chlorophyll).

For each grid cell (x, y) and calendar month m, we computed a per-pixel RMSE of surface chlorophyll using all available daily matchups within that month. To account for the strongly skewed distribution of chlorophyll, all comparisons were performed in $\log_{10}$ space,

$$e_d(m, x, y) = \log_{10}\big(C_d^{\mathrm{mod}}(m, x, y) + \varepsilon\big) - \log_{10}\big(C_d^{\mathrm{obs}}(m, x, y) + \varepsilon\big), \tag{1}$$

where ε is a small constant to avoid $\log_{10}(0)$. The monthly per-pixel RMSE was then defined as

$$\mathrm{RMSE}(m,x,y) = \sqrt{\frac{1}{N(m,x,y)} \sum_{d=1}^{N(m,x,y)} e_d(m,x,y)^2}, \tag{2}$$

with $N(m,x,y)$ denoting the number of valid daily matchups (a minimum sample threshold was applied, and land points were masked using the satellite product).

To evaluate HYB-SF, HYB-PI, legacy ERSEM, and AMM15, we used ESA Ocean Colour CCI chlorophyll as the reference. For the reanalysis comparison, we used the CMEMS ocean-colour product. This ensures the data matches what the reanalysis system used for validation.

Mean bias.

We used mean bias to identify systematic offsets in oxygen and nitrate. We calculated the bias for each grid cell (x,y) and season s as the mean difference between the model and the reference product,

$$\mathrm{Bias}(s,x,y) = \frac{1}{N(s,x,y)} \sum_{d=1}^{N(s,x,y)} \left(C_d^{\mathrm{mod}}(s,x,y) - C_d^{\mathrm{ref}}(s,x,y)\right), \tag{3}$$

where C_d^{mod} and C_d^{ref} denote the modelled and reference tracer concentrations, respectively, s denotes the season (DJF, MAM, JJA, SON), and $N(s,x,y)$ is the number of valid samples. For oxygen and nitrate, HYB-SF, HYB-PI, legacy, and reanalysis simulations were evaluated against the NSBC climatology after remapping model fields to the NSBC grid using nearest-neighbour interpolation. Seasonal mean biases were then computed for DJF, MAM, JJA, and SON.

Additional methods, validation figures (Fig. S1–S8) and tables (Tables S1–S7) are provided in the Supplementary Information.

Acknowledgements. The authors thank Gennadi Lessin for providing the baseline ERSEM model configuration and associated input files. We acknowledge Dale Partridge for providing the high-resolution AMM15 simulations used for model comparison. We thank Mayra Rodriguez, Ralf Quast, and Roman Shevchuk for their contributions to the generation of the satellite-based primary production dataset. We further acknowledge Matthew Palmer and Tim Smyth for constructive discussions and institutional support during the development of this work.

Declarations

- **Funding**
  This work was carried out at Plymouth Marine Laboratory (PML) and supported by institutional research funding and UK National Capability funding through the National Centre for Earth Observation (NCEO). Computational resources were provided through institutional high-performance computing facilities at PML. Methodological developments related to the FABM–Python embedding were supported by the EU-NECCTON project ("New Copernicus Capability for Trophic Ocean Networks"), which received funding from the Horizon Europe Research and Innovation Action programme under Grant Agreement No. 101081273. The generation of the

satellite-based primary production dataset was supported by the European Space Agency project "Satellite-based Observations of Carbon in the Ocean: Pools, Fluxes and Exchanges" (SCOPE). This study also represents a scientific contribution to the UKRI NERC-funded FOCUS project (Grant No. NE/X006271/1). The funders had no role in the study design, model development, analysis, interpretation, or the decision to publish.

- **Competing interests**
  The authors declare no competing interests.
- **Data availability**
  All observational datasets used in this study are publicly available from their respective sources, including ESA Ocean Colour CCI, CMEMS, ICES, BGC-Argo and the NSBC level-2 climatology (see citations in the manuscript). The full-volume NEMO–ERSEM model outputs and intermediate ML training/feature files are large and hosted on HPC storage and are therefore not uploaded in a public repository. To support reproducibility, the processed training and evaluation datasets used to generate the figures and tables (and the trained model artefacts, where applicable) will be archived in an open repository at acceptance. The remaining raw model outputs are available from the corresponding author upon reasonable request.
- **Code availability**
  The code developed for this study (model configuration scripts, ML training/inference code and analysis workflows) is maintained in a private GitHub repository. Read-only access will be provided to editors and peer reviewers during the review process upon request. A public release of the code (or a reproducible subset sufficient to regenerate the main figures and tables) will be archived in a permanent repository at acceptance, subject to institutional and third-party licensing constraints.
- **Author contributions**
  D.S.B. conceived the study, designed and implemented the hybrid modelling framework, performed all simulations, carried out the analysis and validation, and led the writing of the manuscript.
  J.Black. made substantial contributions to the scientific interpretation of the results, critically shaped the structure and framing of the manuscript, and provided detailed feedback throughout the study and contributed to the manuscript.
  G.K. facilitated access to satellite-derived primary production, ocean-colour, and Earth observation datasets used for training and validating the machine-learning components, and provided detailed and constructive feedback that helped refine the results and overall scientific presentation of the manuscript.
  S.S. provided foundational scientific insight and inspiration through extensive conceptual discussions that informed the design of both hybrid approaches and also provided scientific feedback during manuscript review.
  J.Brug. contributed to the technical implementation of the hybrid framework by enabling the integration of the Python-based model within ERSEM via the FABM interface, and provided input on the representation of productivity-rate modifications. He also reviewed and contributed to the manuscript and provided constructive technical and scientific feedback.
  E.M. contributed to the manuscript by sharing insights on policy relevance and societal impact, supported the development of the policy-facing framing of the study, and provided constructive feedback during manuscript review.

H.A.B. reviewed and contributed to the manuscript through critical scientific evaluation and discussion, and provided expertise on the global PI parameter dataset underpinning the physiology-informed hybrid approach.

References

[1] Andrews, O., Buitenhuis, E., Le Quéré, C., Suntharalingam, P.: Biogeochemical modelling of dissolved oxygen in a changing ocean. Phil. Trans. R. Soc. A. **375**(2102), 20160328 (2017) https://doi.org/10.1098/rsta.2016.0328 . Accessed 2026-01-15

[2] Yool, A., Palmiéri, J., Jones, C.G., Mora, L., Kuhlbrodt, T., Popova, E.E., Nurser, A.J.G., Hirschi, J., Blaker, A.T., Coward, A.C., Blockley, E.W., Sellar, A.A.: Evaluating the physical and biogeochemical state of the global ocean component of UKESM1 in CMIP6 historical simulations. Geoscientific Model Development **14**(6), 3437–3472 (2021) https://doi.org/10.5194/gmd-14-3437-2021 . Accessed 2026-01-16

[3] Christian, J.R., Davidson, F., Holdsworth, A.M., Lu, Y., Morgan, J., Zhai, L., Zheng, Z.: A Canada-Wide Ocean Biogeochemical Model Encompassing the North Atlantic, North Pacific and Arctic Oceans. Atmosphere-Ocean **64**(1), 77–99 (2026) https://doi.org/10.1080/07055900.2025.2570153 . _eprint: https://doi.org/10.1080/07055900.2025.2570153. Accessed 2026-01-16

[4] Mamnun, N., Völker, C., Vrekoussis, M., Nerger, L.: Spatially Varying Biogeochemical Parameter Estimation in a Global Ocean Model. JGR Oceans **130**(12), 2025–022752 (2025) https://doi.org/10.1029/2025JC022752 . Accessed 2025-12-15

[5] Skákala, J., Ford, D., Brewin, R.J.W., McEwan, R., Kay, S., Taylor, B., Mora, L., Ciavatta, S.: The Assimilation of Phytoplankton Functional Types for Operational Forecasting in the Northwest European Shelf. Journal of Geophysical Research: Oceans **123**(8), 5230–5247 (2018) https://doi.org/10.1029/2018JC014153 . _eprint: https://agupubs.onlinelibrary.wiley.com/doi/pdf/10.1029/2018JC014153. Accessed 2025-12-10

[6] Ciavatta, S., Torres, R., Martinez-Vicente, V., Smyth, T., Dall'Olmo, G., Polimene, L., Allen, J.I.: Assimilation of remotely-sensed optical properties to improve marine biogeochemistry modelling. Progress in Oceanography **127**, 74–95 (2014) https://doi.org/10.1016/j.pocean.2014.06.002 . Accessed 2026-01-30

[7] Teruzzi, A., Bolzon, G., Salon, S., Lazzari, P., Solidoro, C., Cossarini, G.: Assimilation of coastal and open sea biogeochemical data to improve phytoplankton simulation in the Mediterranean Sea. Ocean Modelling **132**, 46–60 (2018) https://doi.org/10.1016/j.ocemod.2018.09.007 . Accessed 2026-01-30

[8] Gregg, W.W.: Assimilation of SeaWiFS ocean chlorophyll data into a three-dimensional global ocean model. Journal of Marine Systems **69**(3-4), 205–225

(2008) https://doi.org/10.1016/j.jmarsys.2006.02.015 . Accessed 2025-12-10

[9] Mateus, M., Leitão, P.C., Pablo, H., Neves, R.: Is it relevant to explicitly parameterize chlorophyll synthesis in marine ecological models? Journal of Marine Systems **94**(SUPPL.), 23–33 (2012) https://doi.org/10.1016/j.jmarsys.2011.11.007 . Accessed 2025-12-10

[10] Stock, C.A., Dunne, J.P., Luo, J.Y., Ross, A.C., Van Oostende, N., Zadeh, N., Cordero, T.J., Liu, X., Teng, Y.-C.: Photoacclimation and Photoadaptation Sensitivity in a Global Ocean Ecosystem Model. Journal of Advances in Modeling Earth Systems **17**(6), 2024–004701 (2025) https://doi.org/10.1029/2024MS004701 . _eprint: https://agupubs.onlinelibrary.wiley.com/doi/pdf/10.1029/2024MS004701. Accessed 2025-12-10

[11] Siegel, D.A., Buesseler, K.O., Behrenfeld, M.J., Benitez-Nelson, C.R., Boss, E., Brzezinski, M.A., Burd, A., Carlson, C.A., D'Asaro, E.A., Doney, S.C., Perry, M.J., Stanley, R.H.R., Steinberg, D.K.: Prediction of the Export and Fate of Global Ocean Net Primary Production: The EXPORTS Science Plan. Front. Mar. Sci. **3** (2016) https://doi.org/10.3389/fmars.2016.00022 . Accessed 2025-12-10

[12] Skákala, J., Bruggeman, J., Ford, D., Wakelin, S., Akpınar, A., Hull, T., Kaiser, J., Loveday, B.R., O'Dea, E., Williams, C.A.J., Ciavatta, S.: The impact of ocean biogeochemistry on physics and its consequences for modelling shelf seas. Ocean Modelling **172**, 101976 (2022) https://doi.org/10.1016/j.ocemod.2022.101976 . Accessed 2025-12-10

[13] Kay, S., McEwan, R., Ford, D.: NWSHELF_MULTIYEAR_BGC_004_011: North West European Shelf Ocean Biogeochemistry Reanalysis. Copernicus Marine Service (CMEMS), Marine Data Store. Accessed via Copernicus Marine Data Store (2016). https://doi.org/10.48670/moi-00058

[14] Seppi, M., Linnosmaa, J., Zeb, A.: Physics-informed machine learning surrogate models: Enhancing data-driven forecasting for digital twins in mineral processing. Minerals Engineering **230**, 109424 (2025) https://doi.org/10.1016/j.mineng.2025.109424 . Accessed 2025-12-10

[15] Niu, Z., Wang, D., Mu, M., Huang, W., Fan, X., Yang, M., Qin, B.: Machine-Learning (ML)-Physics Fusion Model Accelerates the Paradigm Shift in Typhoon Forecasting With a CNOP-Based Assimilation Framework. Geophysical Research Letters **52**(15), 2025–115926 (2025) https://doi.org/10.1029/2025GL115926 . _eprint: https://agupubs.onlinelibrary.wiley.com/doi/pdf/10.1029/2025GL115926. Accessed 2025-12-10

[16] Kashinath, K., Mustafa, M., Albert, A., Wu, J.-L., Jiang, C., Esmaeilzadeh, S., Azizzadenesheli, K., Wang, R., Chattopadhyay, A., Singh, A., Manepalli, A., Chirila, D., Yu, R., Walters, R., White, B., Xiao, H., Tchelepi, H.A., Marcus, P., Anandkumar, A., Hassanzadeh, P., Prabhat: Physics-informed machine learning:

case studies for weather and climate modelling. Philos Trans A Math Phys Eng Sci **379**(2194), 20200093 (2021) https://doi.org/10.1098/rsta.2020.0093 . Accessed 2025-12-10

[17] Spillias, S.: A Prospectus on Generative Artificial Intelligence in Marine Ecosystem Modelling. Fish and Fisheries **n/a**(n/a) https://doi.org/10.1111/faf.70037 . _eprint: https://onlinelibrary.wiley.com/doi/pdf/10.1111/faf.70037. Accessed 2026-01-29

[18] Rubbens, P., Brodie, S., Cordier, T., Destro Barcellos, D., Devos, P., Fernandes-Salvador, J.A., Fincham, J.I., Gomes, A., Handegard, N.O., Howell, K., Jamet, C., Kartveit, K.H., Moustahfid, H., Parcerisas, C., Politikos, D., Sauzède, R., Sokolova, M., Uusitalo, L., Van den Bulcke, L., van Helmond, A.T.M., Watson, J.T., Welch, H., Beltran-Perez, O., Chaffron, S., Greenberg, D.S., Kühn, B., Kiko, R., Lo, M., Lopes, R.M., Möller, K.O., Michaels, W., Pala, A., Romagnan, J.-B., Schuchert, P., Seydi, V., Villasante, S., Malde, K., Irisson, J.-O.: Machine learning in marine ecology: an overview of techniques and applications. ICES J Mar Sci **80**(7), 1829–1853 (2023) https://doi.org/10.1093/icesjms/fsad100 . Accessed 2026-02-02

[19] Baretta, J.W., Ebenhöh, W., Ruardij, P.: The European regional seas ecosystem model, a complex marine ecosystem model. Netherlands Journal of Sea Research **33**(3), 233–246 (1995) https://doi.org/10.1016/0077-7579(95)90047-0 . Accessed 2025-12-10

[20] Butenschön, M., Clark, J., Aldridge, J.N., Allen, J.I., Artioli, Y., Blackford, J., Bruggeman, J., Cazenave, P., Ciavatta, S., Kay, S., Lessin, G., Leeuwen, S., der Molen, J., Mora, L., Polimene, L., Sailley, S., Stephens, N., Torres, R.: ERSEM 15.06: a generic model for marine biogeochemistry and the ecosystem dynamics of the lower trophic levels. Geoscientific Model Development **9**(4), 1293–1339 (2016) https://doi.org/10.5194/gmd-9-1293-2016 . Publisher: Copernicus GmbH. Accessed 2025-12-10

[21] Sathyendranath, S., Platt, T., Kovač, , Dingle, J., Jackson, T., Brewin, R.J.W., Franks, P., Marañón, E., Kulk, G., Bouman, H.A.: Reconciling models of primary production and photoacclimation [Invited]. Appl. Opt., AO **59**(10), 100–114 (2020) https://doi.org/10.1364/AO.386252 . Publisher: Optica Publishing Group. Accessed 2025-12-10

[22] Kulk, G., Platt, T., Dingle, J., Jackson, T., Jönsson, B.F., Bouman, H.A., Babin, M., Brewin, R.J.W., Doblin, M., Estrada, M., Figueiras, F.G., Furuya, K., González-Benítez, N., Gudfinnsson, H.G., Gudmundsson, K., Huang, B., Isada, T., Kovač, , Lutz, V.A., Marañón, E., Raman, M., Richardson, K., Rozema, P.D., Poll, W.H.v.d., Segura, V., Tilstone, G.H., Uitz, J., Dongen-Vogels, V.v., Yoshikawa, T., Sathyendranath, S., Kulk, G., Platt, T., Dingle, J., Jackson, T., Jönsson, B.F., Bouman, H.A., Babin, M., Brewin, R.J.W., Doblin, M., Estrada, M., Figueiras, F.G., Furuya, K., González-Benítez, N., Gudfinnsson, H.G., Gudmundsson, K., Huang, B., Isada, T., Kovač, , Lutz, V.A., Marañón, E., Raman, M., Richardson, K., Rozema, P.D., Poll, W.H.v.d., Segura, V., Tilstone,

G.H., Uitz, J., Dongen-Vogels, V.v., Yoshikawa, T., Sathyendranath, S.: Primary Production, an Index of Climate Change in the Ocean: Satellite-Based Estimates over Two Decades. Remote Sensing **12**(5) (2020) https://doi.org/10.3390/rs12050826 . Company: Multidisciplinary Digital Publishing Institute Distributor: Multidisciplinary Digital Publishing Institute Institution: Multidisciplinary Digital Publishing Institute Label: Multidisciplinary Digital Publishing Institute Publisher: publisher. Accessed 2025-12-10

[23] Smyth, T.J., Tilstone, G.H., Groom, S.B.: Integration of radiative transfer into satellite models of ocean primary production. Journal of Geophysical Research: Oceans **110**(C10) (2005) https://doi.org/10.1029/2004JC002784 . _eprint: https://agupubs.onlinelibrary.wiley.com/doi/pdf/10.1029/2004JC002784. Accessed 2025-12-10

[24] Natural Environment Research Council: Detection and Attribution of Regional Greenhouse Gas Emissions in the UK (DARE-UK). NERC Reference Number: NE/S004947/1; Grant Stage: Completed; Grant Status: Closed (202?). https://gotw.nerc.ac.uk/list_full.asp?pcode=NE/S004947/1

[25] Bouman, H.A., Platt, T., Doblin, M., Figueiras, F.G., Gudmundsson, K., Gudfinnsson, H.G., Huang, B., Hickman, A., Hiscock, M., Jackson, T., Lutz, V.A., Mélin, F., Rey, F., Pepin, P., Segura, V., Tilstone, G.H., Dongen-Vogels, V., Sathyendranath, S.: Photosynthesis–irradiance parameters of marine phytoplankton: synthesis of a global data set. Earth System Science Data **10**(1), 251–266 (2018) https://doi.org/10.5194/essd-10-251-2018 . Publisher: Copernicus GmbH. Accessed 2025-12-10

[26] Pace, M.L., Lovett, G.M., Carey, C.C., Thomas, R.Q.: Primary production: the foundation of ecosystems. In: Fundamentals of Ecosystem Science, pp. 29–53. Elsevier, ??? (2021)

[27] Schlenger, A.J., Libralato, S., Ballance, L.T.: Temporal Variability of Primary Production Explains Marine Ecosystem Structure and Function. Ecosystems **22**(2), 331–345 (2019) https://doi.org/10.1007/s10021-018-0272-y . Accessed 2025-12-11

[28] Hinrichs, I., Gouretski, V., Pätsch, J., Emeis, K.-C., Stammer, D.: North Sea Biogeochemical Climatology (Version 1.1). World Data Center for Climate (WDCC) at DKRZ. Data set, monthly and climatological fields 1960–2014 for North Sea biogeochemical parameters, accessed 11 December 2025 (2017). https://doi.org/10.1594/WDCC/NSBClim_v1.1

[29] Sathyendranath, S., Brewin, R.J.W., Brockmann, C., Brotas, V., Calton, B., Chuprin, A., Cipollini, P., Couto, A.B., Dingle, J., Doerffer, R., Donlon, C., Dowell, M., Farman, A., Grant, M., Groom, S., Horseman, A., Jackson, T., Krasemann, H., Lavender, S., Martinez-Vicente, V., Mazeran, C., Mélin, F., Moore, T.S., Müller, D., Regner, P., Roy, S., Steele, C.J., Steinmetz, F., Swinton, J., Taberner, M., Thompson, A., Valente, A., Zühlke, M., Brando, V.E., Feng, H., Feldman, G., Franz, B.A., Frouin, R., Gould, R.W., Hooker, S.B., Kahru,

M., Kratzer, S., Mitchell, B.G., Muller-Karger, F.E., Sosik, H.M., Voss, K.J., Werdell, J., Platt, T., Sathyendranath, S., Brewin, R.J.W., Brockmann, C., Brotas, V., Calton, B., Chuprin, A., Cipollini, P., Couto, A.B., Dingle, J., Doerffer, R., Donlon, C., Dowell, M., Farman, A., Grant, M., Groom, S., Horseman, A., Jackson, T., Krasemann, H., Lavender, S., Martinez-Vicente, V., Mazeran, C., Mélin, F., Moore, T.S., Müller, D., Regner, P., Roy, S., Steele, C.J., Steinmetz, F., Swinton, J., Taberner, M., Thompson, A., Valente, A., Zühlke, M., Brando, V.E., Feng, H., Feldman, G., Franz, B.A., Frouin, R., Gould, R.W., Hooker, S.B., Kahru, M., Kratzer, S., Mitchell, B.G., Muller-Karger, F.E., Sosik, H.M., Voss, K.J., Werdell, J., Platt, T.: An Ocean-Colour Time Series for Use in Climate Studies: The Experience of the Ocean-Colour Climate Change Initiative (OC-CCI). Sensors **19**(19) (2019) https://doi.org/10.3390/s19194285 . Company: Multidisciplinary Digital Publishing Institute Distributor: Multidisciplinary Digital Publishing Institute Institution: Multidisciplinary Digital Publishing Institute Label: Multidisciplinary Digital Publishing Institute Publisher: publisher. Accessed 2025-12-10

[30] European Space Agency: Ocean Colour Climate Change Initiative (CCI), Version 6.0. https://climate.esa.int/en/projects/ocean-colour/. Merged multi-sensor Level-3 daily ocean-colour product, 1 km resolution. Accessed: 15 December 2025 (2022)

[31] Wong, A.P.S., Wijffels, S.E., Riser, S.C., Pouliquen, S., Hosoda, S., Roemmich, D., Gilson, J., Johnson, G.C., Martini, K., Murphy, D.J., Scanderbeg, M., Bhaskar, T.V.S.U., Buck, J.J.H., Merceur, F., Carval, T., Maze, G., Cabanes, C., André, X., Poffa, N., Yashayaev, I., Barker, P.M., Guinehut, S., Belbéoch, M., Ignaszewski, M., Baringer, M.O., Schmid, C., Lyman, J.M., McTaggart, K.E., Purkey, S.G., Zilberman, N., Alkire, M.B., Swift, D., Owens, W.B., Jayne, S.R., Hersh, C., Robbins, P., West-Mack, D., Bahr, F., Yoshida, S., Sutton, P.J.H., Cancouët, R., Coatanoan, C., Dobbler, D., Juan, A.G., Gourrion, J., Kolodziejczyk, N., Bernard, V., Bourlès, B., Claustre, H., D'Ortenzio, F., Le Reste, S., Le Traon, P.-Y., Rannou, J.-P., Saout-Grit, C., Speich, S., Thierry, V., Verbrugge, N., Angel-Benavides, I.M., Klein, B., Notarstefano, G., Poulain, P.-M., Vélez-Belchí, P., Suga, T., Ando, K., Iwasaska, N., Kobayashi, T., Masuda, S., Oka, E., Sato, K., Nakamura, T., Sato, K., Takatsuki, Y., Yoshida, T., Cowley, R., Lovell, J.L., Oke, P.R., Wijk, E.M., Carse, F., Donnelly, M., Gould, W.J., Gowers, K., King, B.A., Loch, S.G., Mowat, M., Turton, J., Rama Rao, E.P., Ravichandran, M., Freeland, H.J., Gaboury, I., Gilbert, D., Greenan, B.J.W., Ouellet, M., Ross, T., Tran, A., Dong, M., Liu, Z., Xu, J., Kang, K., Jo, H., Kim, S.-D., Park, H.-M.: Argo Data 1999–2019: Two Million Temperature-Salinity Profiles and Subsurface Velocity Observations From a Global Array of Profiling Floats. Front. Mar. Sci. **7** (2020) https://doi.org/10.3389/fmars.2020.00700 . Publisher: Frontiers. Accessed 2025-12-10

[32] Sea (ICES), I.C.: ICES Data Portal. https://data.ices.dk/. Accessed: 15 December 2025 (2025)

[33] Partridge, D., Berthou, S., Millington, R., Clark, J., Bricheno, L., Castillo, J.M., Rulent, J., Lewis, H.: Impact of waves on phytoplankton activity on the Northwest

European Shelf: insights from observations and km-scale coupled models. EGUsphere, 1–32 (2025) https://doi.org/10.5194/egusphere-2025-3654 . Publisher: Copernicus GmbH. Accessed 2025-12-15

[34] Ferreira, A.S., Visser, A.W., MacKenzie, B.R., Payne, M.R.: Accuracy and precision in the calculation of phenology metrics. Journal of Geophysical Research: Oceans **119**(12), 8438–8453 (2014) https://doi.org/10.1002/2014JC010323 . _eprint: https://agupubs.onlinelibrary.wiley.com/doi/pdf/10.1002/2014JC010323. Accessed 2026-01-08

[35] Jardine, J.E., Palmer, M., Mahaffey, C., Holt, J., Wakelin, S., Artioli, Y.: Climatic Controls on the Spring Phytoplankton Growing Season in a Temperate Shelf Sea. Journal of Geophysical Research: Oceans **127**(5), 2021–017209 (2022) https://doi.org/10.1029/2021JC017209 . _eprint: https://agupubs.onlinelibrary.wiley.com/doi/pdf/10.1029/2021JC017209. Accessed 2025-12-11

[36] Skákala, J., Ford, D., Bruggeman, J., Hull, T., Kaiser, J., King, R.R., Loveday, B., Palmer, M.R., Smyth, T., Williams, C.A.J., Ciavatta, S.: Towards a Multi-Platform Assimilative System for North Sea Biogeochemistry. Journal of Geophysical Research: Oceans **126**(4), 2020–016649 (2021) https://doi.org/10.1029/2020JC016649 . _eprint: https://agupubs.onlinelibrary.wiley.com/doi/pdf/10.1029/2020JC016649. Accessed 2025-12-11

[37] Ciavatta, S., Brewin, R.J.W., Skákala, J., Polimene, L., Mora, L., Artioli, Y., Allen, J.I.: Assimilation of Ocean-Color Plankton Functional Types to Improve Marine Ecosystem Simulations. Journal of Geophysical Research: Oceans **123**(2), 834–854 (2018) https://doi.org/10.1002/2017JC013490 . _eprint: https://agupubs.onlinelibrary.wiley.com/doi/pdf/10.1002/2017JC013490. Accessed 2026-01-19

[38] Best, M.A., Wither, A.W., Coates, S.: Dissolved oxygen as a physico-chemical supporting element in the Water Framework Directive. Marine Pollution Bulletin **55**(1), 53–64 (2007) https://doi.org/10.1016/j.marpolbul.2006.08.037 . Accessed 2026-01-27

[39] OSPAR Commission: OSPAR and the Marine Strategy Framework Directive (MSFD). https://www.ospar.org/work-areas/cross-cutting-issues/msfd. Accessed: YYYY-MM-DD (2023)

[40] OSPAR Commission: OSPAR Quality Status Report 2023. https://oap.ospar.org/en/ospar-assessments/quality-status-reports/qsr-2023/. Accessed: YYYY-MM-DD (2023)

[41] Copernicus Marine Service: OCEANCOLOUR_ATL_BGC_L4_MY_009_118: Atlantic Ocean Colour Biogeochemical L4 Multi-Year Product. https://data.marine.copernicus.eu/product/OCEANCOLOUR_ATL_BGC_L4_MY_009_118.

Accessed: 15 December 2025 (2025)

[42] Brewin, R.J.W., Ciavatta, S., Sathyendranath, S., Jackson, T., Tilstone, G., Curran, K., Airs, R.L., Cummings, D., Brotas, V., Organelli, E., Dall'Olmo, G., Raitsos, D.E.: Uncertainty in Ocean-Color Estimates of Chlorophyll for Phytoplankton Groups. Front. Mar. Sci. **4** (2017) https://doi.org/10.3389/fmars.2017.00104 . Accessed 2026-02-01

[43] Ciavatta, S., Kay, S., Saux-Picart, S., Butenschön, M., Allen, J.I.: Decadal reanalysis of biogeochemical indicators and fluxes in the North West European shelf-sea ecosystem. Journal of Geophysical Research: Oceans **121**(3), 1824–1845 (2016) https://doi.org/10.1002/2015JC011496 . _eprint: https://agupubs.onlinelibrary.wiley.com/doi/pdf/10.1002/2015JC011496. Accessed 2025-12-11

[44] Tonani, M., Sykes, P., King, R.R., McConnell, N., Péquignet, A.-C., O'Dea, E., Graham, J.A., Polton, J., Siddorn, J.: The impact of a new high-resolution ocean model on the Met Office North-West European Shelf forecasting system. Ocean Science **15**(4), 1133–1158 (2019) https://doi.org/10.5194/os-15-1133-2019 . Publisher: Copernicus GmbH. Accessed 2025-12-10

[45] Flynn, K.J., Atkinson, A., Beardall, J., Berges, J.A., Boersma, M., Brunet, C., Calbet, A., Caron, D.A., Dam, H.G., Glibert, P.M., Hansen, P.J., Jin, P., Lønborg, C., Mayor, D.J., Menden-Deuer, S., Mock, T., Mulholland, M.R., Needham, D.M., Polimene, L., Poulton, A.J., Robinson, C., Rokitta, S.D., Rost, B., Saiz, E., Scanlan, D.J., Schmidt, K., Sherr, E., Stoecker, D.K., Svensen, C., Thiele, S., Thingstad, T.F., Våge, S.: More realistic plankton simulation models will improve projections of ocean ecosystem responses to global change. Nat Ecol Evol **9**(9), 1562–1570 (2025) https://doi.org/10.1038/s41559-025-02788-3 . Accessed 2026-02-01

[46] Banerjee, D.S., Skakala, J., Ford, D.: Combining machine learning with data assimilation to improve the quality of phytoplankton forecasting in a shelf sea environment. arXiv. arXiv:2508.02400 [q-bio] (2025). https://doi.org/10.48550/arXiv.2508.02400 . http://arxiv.org/abs/2508.02400 Accessed 2025-12-11

[47] Banerjee, D.S., Skákala, J.: Improved understanding of nitrate trends, eutrophication indicators, and risk areas using machine learning. Biogeosciences **22**(15), 3769–3784 (2025) https://doi.org/10.5194/bg-22-3769-2025 . Publisher: Copernicus GmbH. Accessed 2025-12-11

[48] Ehlers, S., Hoffmann, N., Tang, T., Callaghan, A.H., Cao, R., Padilla, E.M., Fang, Y., Stender, M.: Physics-informed neural networks for phase-resolved data assimilation and prediction of nonlinear ocean waves. Phys. Rev. Fluids **10**(9), 094901 (2025) https://doi.org/10.1103/ytyy-pvys . Accessed 2026-01-21

[49] Bang, C., Altaher, A.S., Zhuang, H., Altaher, A., Srinivasan, A., Chérubin, L.M.: Physics-informed neural networks to reconstruct surface velocity field from drifter data. Front. Mar. Sci. **12** (2025) https://doi.org/10.3389/fmars.2025.1547995 .

Accessed 2026-01-21

[50] Yuan, T., Zhu, J., Wang, W., Lu, J., Wang, X., Li, X., Ren, K.: A Space-Time Partial Differential Equation Based Physics-Guided Neural Network for Sea Surface Temperature Prediction. Remote Sensing **15**(14) (2023) https://doi.org/10.3390/rs15143498 . Accessed 2026-01-21

[51] Park, J.-S., Park, J.-Y., Ham, Y.-G., Kim, J.-H., Jeon, W.J.: A Deep Learning Framework for Chlorophyll Prediction in Large Marine Ecosystems: Benchmarking with a Dynamic Model and Implications for Fish Catch Forecasts. EGUsphere, 1–19 (2025) https://doi.org/10.5194/egusphere-2025-5673 . Accessed 2026-01-30

[52] Sane, A., Reichl, B.G., Adcroft, A., Zanna, L.: Parameterizing Vertical Mixing Coefficients in the Ocean Surface Boundary Layer Using Neural Networks. Journal of Advances in Modeling Earth Systems **15**(10), 2023–003890 (2023) https://doi.org/10.1029/2023MS003890 . _eprint: https://agupubs.onlinelibrary.wiley.com/doi/pdf/10.1029/2023MS003890. Accessed 2026-01-27

[53] Galli, G., Wakelin, S., Harle, J., Holt, J., Artioli, Y.: Multi-model comparison of trends and controls of near-bed oxygen concentration on the northwest European continental shelf under climate change. Biogeosciences **21**(8), 2143–2158 (2024) https://doi.org/10.5194/bg-21-2143-2024 . Publisher: Copernicus GmbH. Accessed 2025-12-11

[54] Wakelin, S.L., Artioli, Y., Holt, J.T., Butenschön, M., Blackford, J.: Controls on near-bed oxygen concentration on the Northwest European Continental Shelf under a potential future climate scenario. Progress in Oceanography **187**, 102400 (2020) https://doi.org/10.1016/j.pocean.2020.102400 . Accessed 2025-12-11

[55] A pro-innovation approach to AI regulation. https://www.gov.uk/government/publications/ai-regulation-a-pro-innovation-approach/white-paper Accessed 2025-12-10

[56] Department for Environment, Food Rural Affairs (DEFRA): DEFRA Digital Sustainability Strategy 2025 to 2030. UK Government. Accessed: 2026-01-15. https://www.gov.uk/government/publications/defra-digital-sustainability-strategy-2025-to-2030/defra-digital-sustainability-strategy-2025-to-2030

[57] AI Act | Shaping Europe's digital future (2025). https://digital-strategy.ec.europa.eu/en/policies/regulatory-framework-ai Accessed 2025-12-10

[58] Participation, E.: Fisheries Act 2020. Statute Law Database. https://www.legislation.gov.uk/ukpga/2020/22/contents Accessed 2026-01-27

[59] Goal 14 | Department of Economic and Social Affairs. https://sdgs.un.org/goals/goal14 Accessed 2026-01-27

[60] Department for Energy Security and Net Zero: Impact of growth of data

centres on energy consumption. https://www.gov.uk/government/publications/impact-of-growth-of-data-centres-on-energy-consumption. Published 14 August 2025; Accessed 11 December 2025 (2025)

[61] Gurvan, M., Bourdallé-Badie, R., Bouttier, P.-A., Bricaud, C., Bruciaferri, D., Calvert, D., Chanut, J., Clementi, E., Coward, A., Delrosso, D., Ethé, C., Flavoni, S., Graham, T., Harle, J., Iovino, D., Lea, D., Lévy, C., Lovato, T., Martin, N., Masson, S., Mocavero, S., Paul, J., Rousset, C., Storkey, D., Storto, A., Vancoppenolle, M.: NEMO ocean engine (2017) https://doi.org/10.5281/zenodo.3248739 . Publisher: Zenodo. Accessed 2025-12-10

[62] Bruggeman, J., Bolding, K.: A general framework for aquatic biogeochemical models. Environmental Modelling & Software **61**, 249–265 (2014) https://doi.org/10.1016/j.envsoft.2014.04.002 . Accessed 2025-12-10

[63] Skákala, J., Bruggeman, J., Brewin, R.J.W., Ford, D.A., Ciavatta, S.: Improved Representation of Underwater Light Field and Its Impact on Ecosystem Dynamics: A Study in the North Sea. Journal of Geophysical Research: Oceans **125**(7), 2020–016122 (2020) https://doi.org/10.1029/2020JC016122 . _eprint: https://agupubs.onlinelibrary.wiley.com/doi/pdf/10.1029/2020JC016122. Accessed 2025-12-10

[64] Ford, D., Kay, S., McEwan, R., Totterdell, I., Gehlen, M.: Marine Biogeochemical Modelling and Data Assimilation for Operational Forecasting, Reanalysis, and Climate Research. In: Chassignet, E.P., Pascual, A., Tintoré, J., Verron, J. (eds.) New Frontiers in Operational Oceanography. GODAE OceanView, ??? (2018). https://doi.org/10.17125/gov2018.ch22 . http://purl.flvc.org/fsu/fd/FSU$_l ibsubv1_s cholarship_s ubmission_1 536246093_2 a451821 Accessed 2025-12-10

[65] O'Dea, E., Furner, R., Wakelin, S., Siddorn, J., While, J., Sykes, P., King, R., Holt, J., Hewitt, H.: The CO5 configuration of the 7 km Atlantic Margin Model: large-scale biases and sensitivity to forcing, physics options and vertical resolution. Geoscientific Model Development **10**(8), 2947–2969 (2017) https://doi.org/10.5194/gmd-10-2947-2017 . Publisher: Copernicus GmbH. Accessed 2025-12-10

[66] Storkey, D., Blockley, E.W., Furner, R., Guiavarc'h, C., Lea, D., Martin, M.J., Barciela, R.M., Hines, A., Hyder, P., Siddorn, J.R.: Forecasting the ocean state using NEMO:The new FOAM system. Journal of Operational Oceanography **3**(1), 3–15 (2010) https://doi.org/10.1080/1755876X.2010.11020109 . Publisher: Taylor & Francis _eprint: https://doi.org/10.1080/1755876X.2010.11020109. Accessed 2025-12-10

[67] Berg, P., Poulsen, J.W.: Implementation Details for HBM. Danish Meteorological Institute, ??? (2012)

[68] Blackford, J.C.: An analysis of benthic biological dynamics in a North Sea ecosystem model. Journal of Sea Research **38**(3), 213–230 (1997) https://doi.org/10.

1016/S1385-1101(97)00044-0 . Accessed 2025-12-10

[69] Rj, G., Hl, M., Tm, K.: Dynamic model of phytoplankton growth and acclimation: responses of the balanced growth rate and the chlorophyll a:carbon ratio to light, nutrient-limitation and temperature. Marine Ecology Progress Series **148**, 187–200 (1997) https://doi.org/10.3354/meps148187 . Accessed 2025-12-10

[70] Artioli, Y., Blackford, J.C., Butenschön, M., Holt, J.T., Wakelin, S.L., Thomas, H., Borges, A.V., Allen, J.I.: The carbonate system in the north sea: Sensitivity and model validation. Journal of Marine Systems **102-104**, 1–13 (2012) https://doi.org/10.1016/j.jmarsys.2012.04.006

[71] Ecological Geography of the Sea, (2010). https://shop.elsevier.com/books/ecological-geography-of-the-sea/longhurst/978-0-12-455521-1 Accessed 2026-01-28

[72] Embury, O., Merchant, C.J., Good, S.A., Rayner, N.A., Høyer, J.L., Atkinson, C., Block, T., Alerskans, E., Pearson, K.J., Worsfold, M., McCarroll, M., Donlon, C.: ESA Sea Surface Temperature Climate Change Initiative (SST_cci): Advanced Very High Resolution Radiometer (AVHRR) Level 2 Pre-processed (L2P) Product, Version 3.0. https://dx.doi.org/10.5285/ec659b31a8ca40918e58ec6d03af07a6. NERC EDS Centre for Environmental Data Analysis. Accessed: 15 December 2025 (2024)

[73] Frouin, R., McPherson, J., Ueyoshi, K., Franz, B.A.: A time series of photosynthetically available radiation at the ocean surface from SeaWiFS and MODIS data. In: Remote Sensing of the Marine Environment II, vol. 8525, pp. 234–245. SPIE, ??? (2012). https://doi.org/10.1117/12.981264 . https://www.spiedigitallibrary.org/conference-proceedings-of-spie/8525/852519/A-time-series-of-photosynthetically-available-radiation-at-the-ocean/10.1117/12.981264.full Accessed 2025-12-10

[74] Copernicus Climate Change Service (C3S): ERA5 hourly data on single levels from 1940 to present. https://cds.climate.copernicus.eu/datasets/reanalysis-era5-single-levels. Copernicus Climate Change Service (C3S) Climate Data Store (CDS), Accessed 11 December 2025 (2023). https://doi.org/10.24381/cds.adbb2d47

[75] Copernicus Marine Service: NWSHELF_MULTIYEAR_PHY_004_009: Atlantic–European North-West Shelf Ocean Physics Reanalysis. https://data.marine.copernicus.eu/product/NWSHELF_MULTIYEAR_PHY_004_009. Accessed: 15 December 2025 (2025)

[76] Forsythe, W.C., Rykiel, E.J., Stahl, R.S., Wu, H.-i., Schoolfield, R.M.: A model comparison for daylength as a function of latitude and day of year. Ecological Modelling **80**(1), 87–95 (1995) https://doi.org/10.1016/0304-3800(94)00034-F . Accessed 2026-01-14

[77] Akiba, T., Sano, S., Yanase, T., Ohta, T., Koyama, M.: Optuna: A Next-generation Hyperparameter Optimization Framework. Proceedings of the 25th ACM SIGKDD International Conference on Knowledge Discovery and Data Mining, 2623–2631 (2019)

[78] Argo Steering Team: Acknowledging Argo Data. https://argo.ucsd.edu/data/acknowledging-argo/. Accessed: 15 December 2025 (2025)

Supplementary Information

Hybrid Physics–AI Ecosystem Simulations Improve Biogeochemical Predictions in Temperate Shelf Seas

Overview

In this document, we present extended validation results to support the findings of our main study. We evaluated the hybrid models against NSBC climatology, independent observations from BGC-Argo floats and ICES profiles. This document also describes the architecture and training strategy of the machine-learning modules integrated into the process-based model (NEMO-ERSEM). Further figures and data tables are provided to offer a complete view of the model's performance and stability.

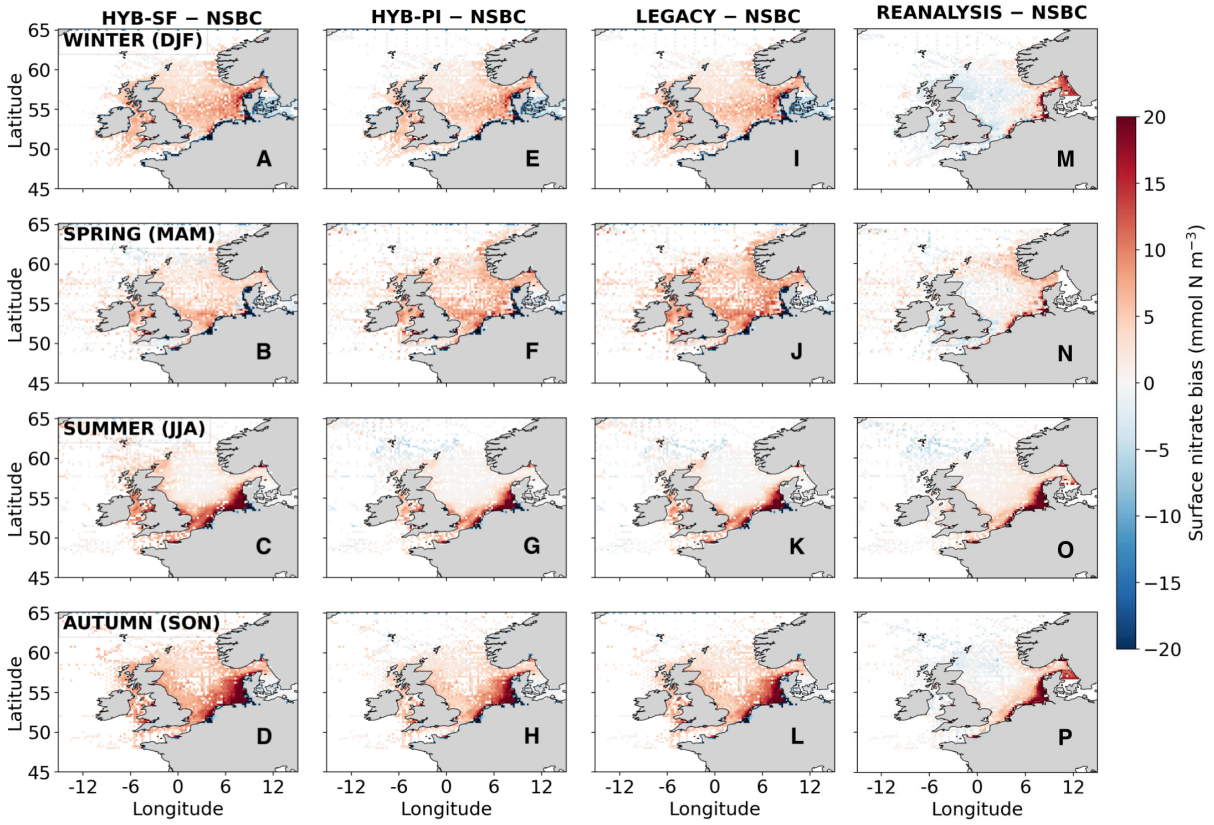

Figure S1: **Seasonal mean (2017-2023) surface nitrate bias for hybrid runs, legacy ERSEM and CMEMS reanalysis against NSBC Level-2 climatology (1960–2014).** Across seasons, all runs showed positive nitrate bias on the shelf when compared with the NSBC climatology. HYB-SF overall lay on the higher side of the bias. This reflects the nutrient-retaining behaviour of ERSEM is shared by all four systems. Although HYB-SF reduced a strong coastal bias along the German–Dutch coastline during spring (panel B), sensitive to nitrate loading and eutrophication pressure.

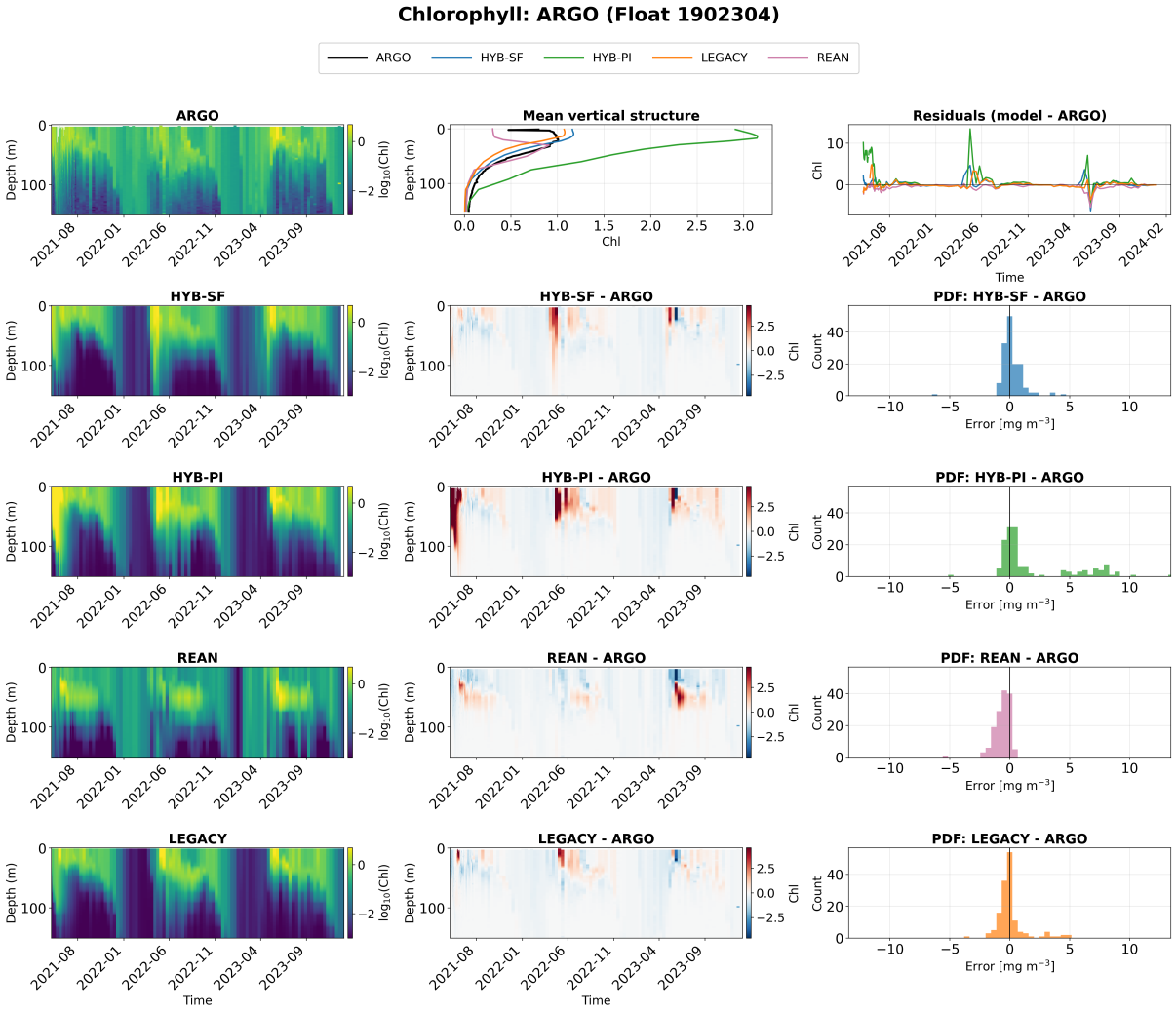

Figure S2: **Validation of simulated chlorophyll against a representative BGC-Argo float (ID 1902304; 48.87°N, 14.85°W).** Panels compare observed BGC-Argo chlorophyll profiles with legacy ERSEM, HYB-SF, HYB-PI simulations and reanalysis. HYB-SF avoided the subsurface chlorophyll overestimation present in the reanalysis and reproduced the observed vertical structure more realistically. HYB-PI overshot the bloom and exhibited a pronounced positive bias in the upper 100 m, resulting in the weakest agreement at this location.

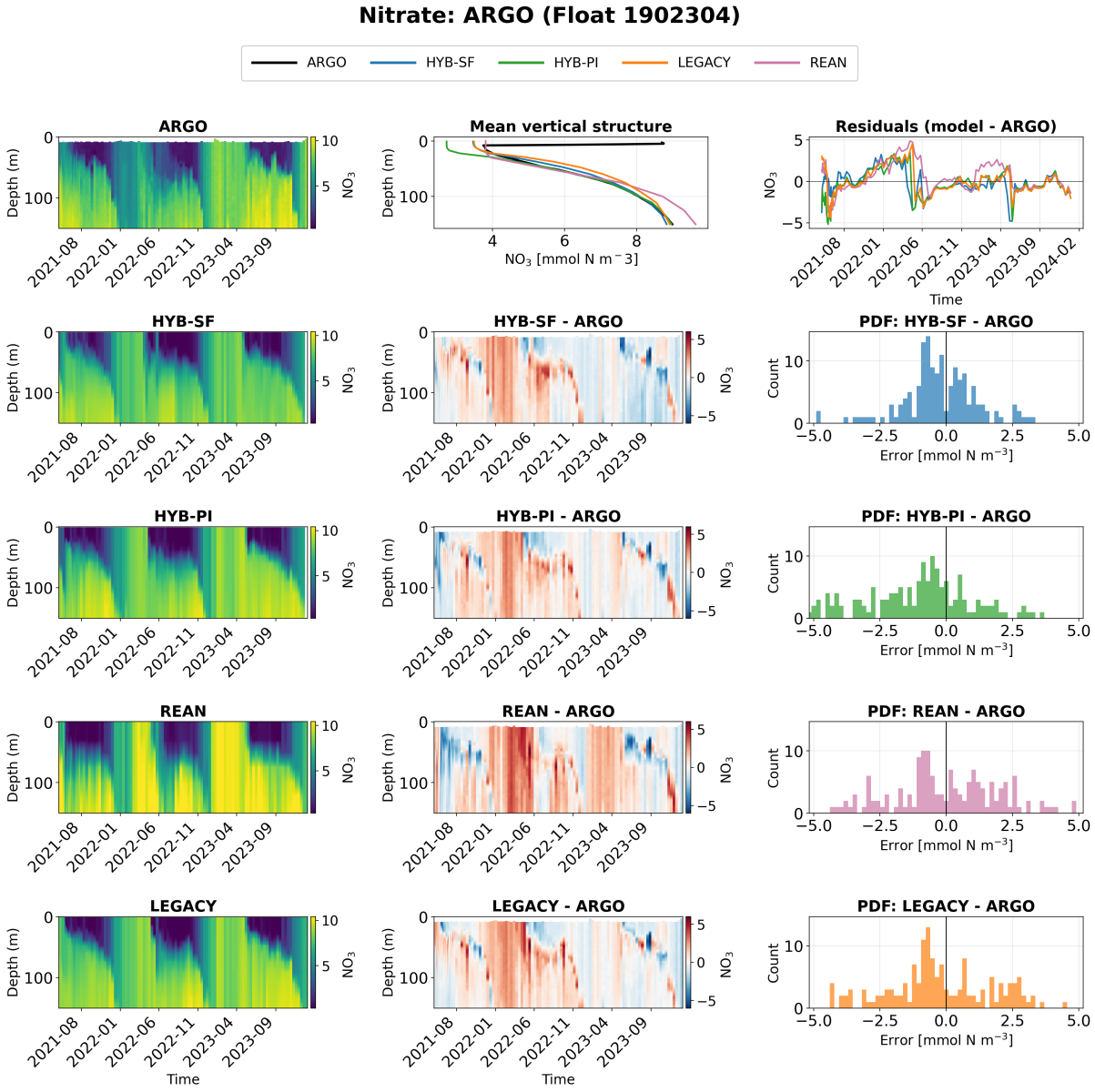

Figure S3: **Validation of simulated nitrate against a representative BGC-Argo float (ID 1902304; 48.87°N, 14.85°W).** Panels compare observed BGC-Argo nitrate profiles with legacy ERSEM, HYB-SF, HYB-PI simulations and reanalysis. HYB-SF showed the closest agreement with observed seasonal nitrate evolution, capturing late-spring drawdown and the vertical structure more consistently than the other configurations. All systems exhibited a post-bloom positive bias, but HYB-SF displayed the narrowest residual distribution centred near zero. HYB-PI showed a broader error spread, while the reanalysis exhibited a systematic positive bias through the water column during the bloom season. Mean profiles indicate that all simulations broadly reproduced the observed structure, with HYB-SF providing the most consistent match down to 150 m.

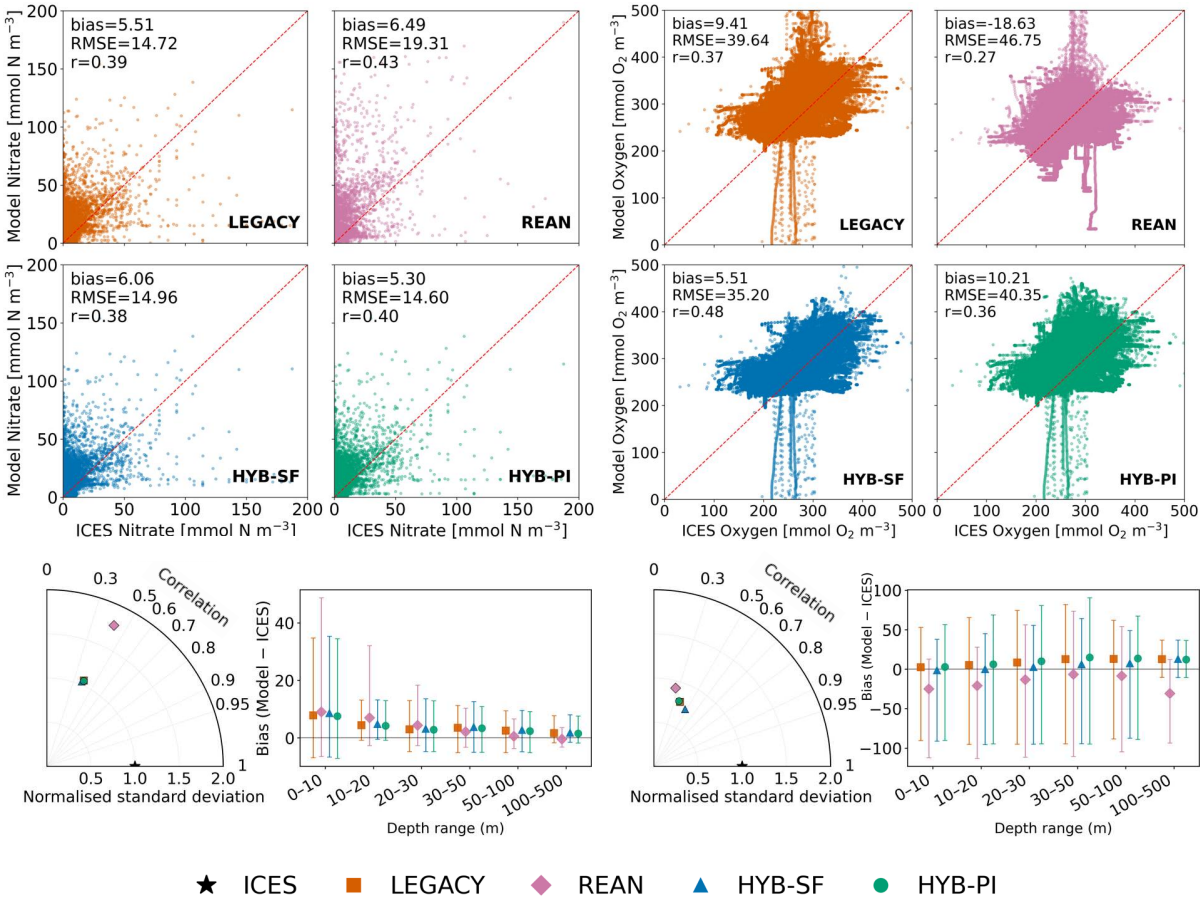

Figure S4: **ICES nitrate and Oxygen validation (2017–2023).** Direct comparison with collocated ICES profiles shows that HYB-PI performed best for nitrate, while HYB-SF performed best for oxygen, exhibiting the lowest bias and smallest RMSE. For nitrate, HYB-PI outperformed HYB-SF, legacy ERSEM, and the reanalysis, which exhibited overestimation and a broad spread of high outliers; HYB-SF largely followed legacy behaviour with modest improvement. For oxygen, HYB-SF showed the highest skill with the lowest RMSE and bias, while the reanalysis exhibited a persistent negative bias from the surface to depth.

Table S1: **Region-wise bias and RMSE for legacy ERSEM, HYB-SF, HYB-PI and AMM15 simulations.** Bold RMSE values indicate improvement relative to AMM15

Region	**Run**	**Bias**	**RMSE**
AMM7	LEGACY	0.05	1.31
	AMM15	0.11	1.20
	HYB-PI	1.09	1.24
	HYB-SF	0.44	**0.91**
Shelf (≤200 m)	LEGACY	−0.06	1.28
	AMM15	−0.16	1.22
	HYB-PI	0.92	**1.16**
	HYB-SF	0.41	**0.83**
Coastal (≤50 m)	LEGACY	−0.84	1.38
	AMM15	−1.18	1.35
	HYB-PI	0.23	**1.24**
	HYB-SF	−0.55	**0.87**
English Channel	LEGACY	−0.47	0.88
	AMM15	−0.67	0.86
	HYB-PI	0.22	0.89
	HYB-SF	−0.55	**0.62**
German Bight	LEGACY	−2.21	1.57
	AMM15	−2.47	1.41
	HYB-PI	−0.65	**1.32**
	HYB-SF	−1.44	**0.94**
Liverpool Bay	LEGACY	−0.98	1.85
	AMM15	−1.01	1.81
	HYB-PI	0.03	**1.70**
	HYB-SF	−0.92	**1.12**

Table S2: **Region-wise chlorophyll bias and RMSE against CMEMS ocean-colour.** Bold RMSE values indicate improvement relative to legacy ERSEM.

Region	Run	Bias ($\mathrm{mg\,m^{-3}}$)	RMSE ($\mathrm{log_{10}\,mg\,m^{-3}}$)
AMM7	REANALYSIS	−0.55	0.57
	LEGACY	−0.02	1.33
	HYB-PI	0.79	**1.30**
	HYB-SF	0.16	**1.02**
Shelf (≤200 m)	REANALYSIS	−0.76	0.58
	LEGACY	−0.27	1.32
	HYB-PI	0.47	**1.25**
	HYB-SF	−0.02	**0.92**
Coastal (≤50 m)	REANALYSIS	−1.61	0.60
	LEGACY	−1.25	1.42
	HYB-PI	−0.54	**1.32**
	HYB-SF	−1.06	**0.95**
English Channel	REANALYSIS	−1.20	0.49
	LEGACY	−0.79	0.90
	HYB-PI	−0.31	0.90
	HYB-SF	−0.69	**0.66**
German Bight	REANALYSIS	−2.76	0.70
	LEGACY	−2.70	1.71
	HYB-PI	−1.93	**1.58**
	HYB-SF	−2.52	**1.23**
Liverpool Bay	REANALYSIS	−1.76	0.68
	LEGACY	−1.75	1.87
	HYB-PI	−1.12	**1.74**
	HYB-SF	−1.63	**1.12**

S1 HYB-PI: Photosynthesis-Irradiance (PI) parameter ML emulator

S1.1 Model training and optimisation:

The hybrid physiological model was trained using a dual-head HistGradientBoostingRegressor to predict the PI parameters α^B and P_m^B. Both parameters were learned at the same time within a single model. The ML-predicted PI parameters were applied uniformly across all four ERSEM phytoplankton functional types (PFTs), replacing the native PFT-specific values with a single dynamically predicted set at each timestep and location. Training was limited to samples with $\alpha^B \leq 0.12$. This resulted in a curated dataset of 2000 observations.

The feature set was physics-guided and had 11 variables in total. These covered geometric harmonics, depth, seasonal forcing, sea-surface temperature, wind mixing, and an irradiance–temperature interaction term. All predictors were passed through the same `StandardScaler`. Hyperparameter tuning was carried out using Optuna, and the final model setup is listed in Table S1.

The trained model shows balanced performance for both parameters. Holdout scores are $R^2 = 0.48$ for α^B and $R^2 = 0.56$ for P_m^B. Cross-validation skill is stable. The 5-fold

mean R^2 values are 0.42 for α^B and 0.56 for P_m^B as shown in Table S2.

Table S3: **Hybrid dual-HGBR model configuration used for learning α^B and P_m^B.** Model trained only on records where $\alpha^B \leq 0.12$. Feature abbreviations denote longitude harmonics (`sin_lon`, `cos_lon`), latitude (`Latitude`), bathymetry (`depth_m`), astronomical daylength (`daylength_h`), seasonal harmonics (`sin_doy`, `cos_doy`), sea-surface temperature (`sst_C`), wind speed (`wind_speed_ms`), photosynthetically active radiation (`PAR_Wm2`), and an irradiance–temperature interaction term (`sst_x_PAR`).

Property	**Value**
Training samples (N)	2000
Feature set (11)	`sin_lon, cos_lon, Latitude, depth_m, daylength_h, sin_doy, cos_doy, sst_C, wind_speed_ms, PAR_Wm2, sst_x_PAR`
Log-transform targets	True
Best Optuna hyperparameters	
Loss function	`absolute_error`
Learning rate	0.08
Maximum iterations	850
Maximum leaf nodes	251
Minimum samples per leaf	23
L2 regularisation	6.25×10^{-6}
Maximum depth	None

S1.2 Performance metrics

Table S4: **Predictive skill of the dual-HGBR hybrid model for α^B and P_m^B.** Holdout metrics correspond to the fixed validation split used in Optuna. Cross-validation (CV) refers to 5-fold shuffled validation using the tuned hyperparameters.

	Holdout		**5-fold CV**	
Metric	α^B	P_m^B	α^B	P_m^B
R^2	0.48	0.56	0.42 ± 0.03	0.56 ± 0.02
MAE	0.011	0.89	0.011 ± 0.0005	0.88 ± 0.027

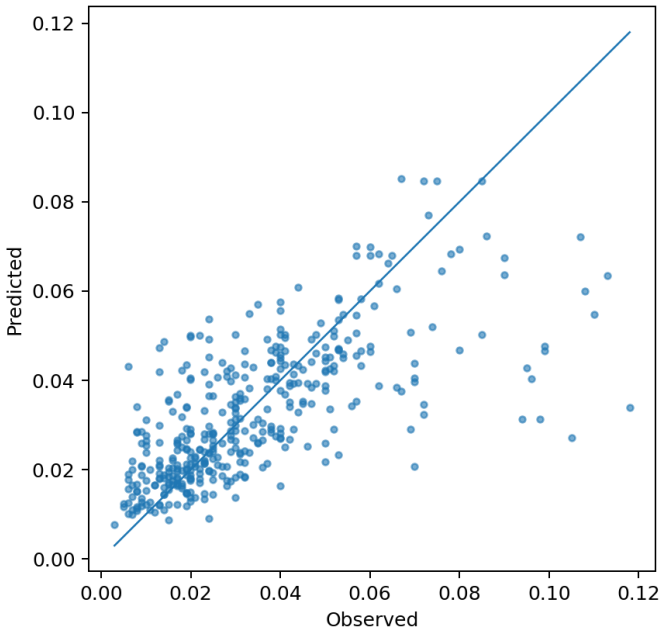

Figure S5: Holdout scatter plot for α^B predictions.

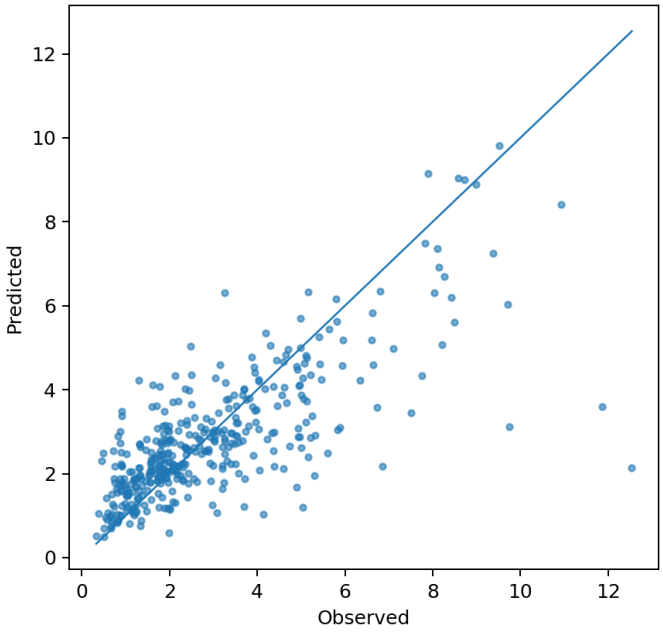

Figure S6: Holdout scatter plot for P_m^B predictions.

S2 HYB-SF: primary productivity scale-factor ML emulator

S2.1 Model training and optimisation:

The HYB-SF setup learned a gross primary production scale factor that linked satellite-based production to the baseline ERSEM production integrated to the euphotic depth. Here, P_{sat} denotes satellite-derived gross primary production, and $P_{mod,zeu}$ denotes ERSEM

gross primary production integrated over the euphotic zone. The model predicts

$$z = \log\left(\frac{\mathrm{P_{sat}}}{\mathrm{P_{mod,zeu}}}\right),$$

using physics-guided surface and bathymetric predictors on the AMM7 grid. The resulting scale factor was applied online within ERSEM as a multiplicative adjustment to the primary production rate. While the correction was applied consistently across all phytoplankton functional types (PFTs), its effective impact was naturally confined to the euphotic zone through ERSEM's depth-resolved light limitation and vertical attenuation, becoming negligible below.

The HYB-SF pathway learned this correction by fitting the ratio between satellite-derived $\mathrm{P_{sat}}$ and ERSEM $\mathrm{P_{mod,zeu}}$. The model was trained only on shelf pixels with valid production during the period 2000–2012. In total, more than 5.6×10^5 monthly grid cells were used for training. The feature set was physics-motivated and includes sea surface temperature, irradiance, wind forcing, salinity, bathymetry, and daylength. It also includes simple interaction terms and a cyclic representation of the annual cycle. Hyperparameters of the HistGradientBoostingRegressor are tuned using Optuna. Optimisation targets R^2 in log space on an independent validation period covering 2013–2014.

The final model explained approximately 83–87 % of the variance in held-out validation and test data (2015) in log space, with R^2 values between 0.83 and 0.87. Performance remained consistent when evaluated in linear space. This indicates that the scale-factor correction was robust and well constrained across the observed range of primary production.

S2.2 Performance metrics

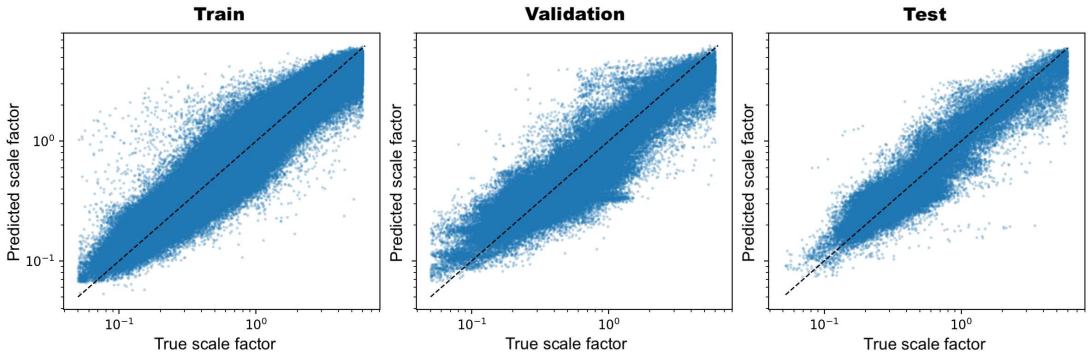

Figure S7: **HYB-SF diagnostics.** Scatter plots of true vs predicted scale factor ($\mathrm{P_{sat}}/\mathrm{P_{mod,zeu}}$) for the train, validation, and test sets in log–log space. The 1:1 (dashed black) line is shown for reference.

Table S5: **Configuration of the HYB-SF scale-factor model.** The target was the logarithm of the Satellite-to-ERSEM primary productivity (PP) ratio $z = \log(\mathrm{P_{sat}}/\mathrm{P_{mod,zeu}})$, trained only on shelf pixels (≤ 200 m) with quality-controlled primary productivity and scale factors between 0.05 and 6.0. The feature set comprises sea-surface temperature (`sst`), photosynthetically active radiation (`par`), 10 m wind speed (`wind10m`), sea-surface salinity (`sss`), longitude and latitude (`lon`, `lat`), bathymetry (`depth`), astronomical daylength (`daylength_h`), daily-integrated irradiance (`par_day`), squared wind speed (`wind2`), logarithmic bathymetry (`log1p_depth`), an irradiance–temperature interaction term (`sst_x_par`), and seasonal harmonics (`month_sin`, `month_cos`).

Property	**Value**
Target	$z = \log(\mathrm{P_{sat}}/\mathrm{P_{mod,zeu}})$
Spatial domain	AMM7 shelf (depth ≤ 200 m)
Temporal coverage	March 2000 – December 2015
Training/validation/test split	Train: $\leq$ 2012; Validation: 2013–2014; Test: 2015
Samples (N)	Train: 561 779; Validation: 92 571; Test: 42 947
Feature set (14)	`sst, par, wind10m, sss, lon, lat, depth, daylength_h, par_day, wind2, log1p_depth, sst_x_par, month_sin, month_cos`
Standardised columns	First 12 numeric features (`numeric_scaled = 12`)
PP filters	$\mathrm{P_{mod,zeu}} \geq 10^{-3}$ mg C m^{-2} d^{-1}; $0.05 \leq$ scale ≤ 6.0
Tail reweighting	Upper 25% of scale distribution upweighted by factor 3.0
Uncertainty handling	`use_uncertainty = True`, `unc_max = 200` (high-uncertainty pixels dropped)
Base learner	`HistGradientBoostingRegressor`
Best Optuna hyperparameters	
Loss function	`squared_error`
Learning rate	0.07
Maximum iterations	301
Maximum leaf nodes	116
Minimum samples per leaf	289
L2 regularisation	3.45×10^{-7}
Maximum depth	9

Table S6: **Performance of HYB-SF in log space** for the target $z = \log(\mathrm{P_{sat}}/\mathrm{P_{mod,zeu}})$. Metrics are mean absolute error (MAE), root-mean-square error (RMSE), and coefficient of determination R^2.

Set	MAE	RMSE	R^2
Train	0.21	0.28	0.92
Validation	0.31	0.41	0.83
Test	0.27	0.35	0.87

Table S7: **Performance of HYB-SF in linear scale** for the PP scale factor scale = $P_{sat}/P_{mod,zeu}$.

Set	MAE	RMSE	R^2
Train	0.21	0.39	0.89
Validation	0.29	0.53	0.80
Test	0.26	0.49	0.83

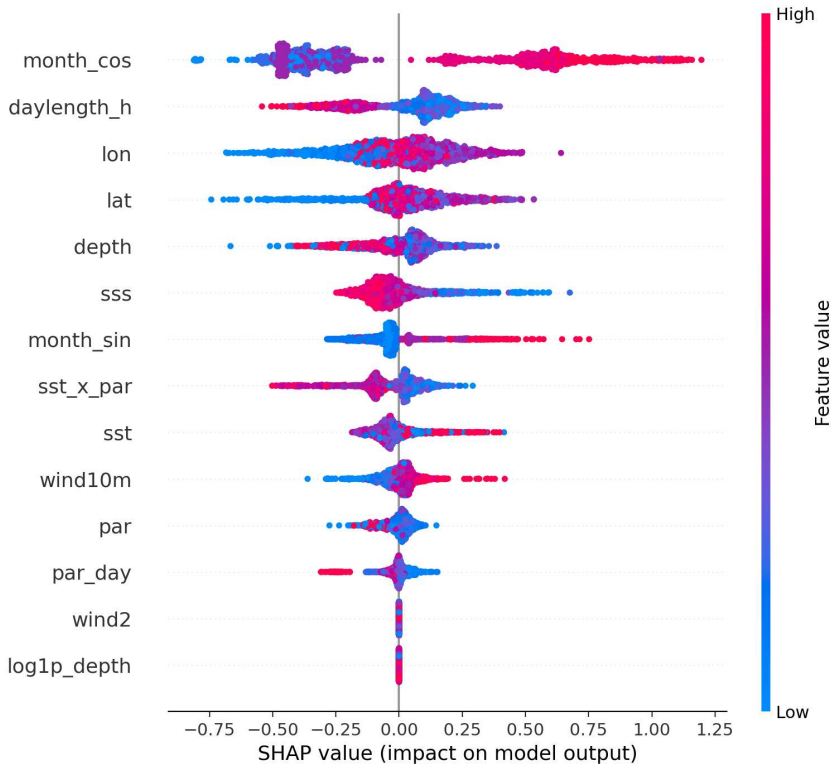

Figure S8: **HYB-SF feature importance from SHAP analysis.** Global SHAP bar plot computed on a subsample of the training data, ranked by absolute mean contribution to the log-scale target $z = \log(P_{sat}/P_{mod,zeu})$.